Helminthic dehydrogenase drives PGE$_2$ and IL-10 production in monocytes to potentiate Treg induction

Ulrich Fabien Prodjinotho[1,2], Vitka Gres[3,†], Fiona Henkel[4,†] (iD), Matthew Lacorcia[1], Ramona Dandl[5] (iD), Martin Haslbeck[5], Veronika Schmidt[2,6,7], Andrea Sylvia Winkler[2,6,7] (iD), Chummy Sikasunge[8] (iD), Per-Johan Jakobsson[9] (iD), Philipp Henneke[3,10,11] (iD), Julia Esser-von Bieren[4] (iD) & Clarissa Prazeres da Costa[1,2,12,*] (iD)

Abstract

Immunoregulation of inflammatory, infection-triggered processes in the brain constitutes a central mechanism to control devastating disease manifestations such as epilepsy. Observational studies implicate the viability of _Taenia solium_ cysts as key factor determining severity of neurocysticercosis (NCC), the most common cause of epilepsy, especially in children, in Sub-Saharan Africa. Viable, in contrast to decaying, cysts mostly remain clinically silent by yet unknown mechanisms, potentially involving Tregs in controlling inflammation. Here, we show that glutamate dehydrogenase from viable cysts instructs tolerogenic monocytes to release IL-10 and the lipid mediator PGE$_2$. These act in concert, converting naive CD4$^+$ T cells into CD127$^-$CD25^{hi}FoxP3$^+$CTLA-4$^+$ Tregs, through the G protein-coupled receptors EP2 and EP4 and the IL-10 receptor. Moreover, while viable cyst products strongly upregulate IL-10 and PGE$_2$ transcription in microglia, intravesicular fluid, released during cyst decay, induces pro-inflammatory microglia and TGF-β as potential drivers of epilepsy. Inhibition of PGE$_2$ synthesis and IL-10 signaling prevents Treg induction by viable cyst products. Harnessing the PGE$_2$-IL-10 axis and targeting TGF-ß signaling may offer an important therapeutic strategy in inflammatory epilepsy and NCC.

Keywords glutamate dehydrogenase; immune regulation; Prostaglandin E2; _Taenia solium_ cyst; Treg cells

Introduction

In chronic helminth infections, the induction of Tregs constitutes an important regulatory mechanism that the parasite utilizes to survive in the immunocompetent host (Maizels _et al_, 2018). Tregs generated during helminth infections control overt inflammatory, and potentially host-destructive immune responses in tissues, but can impair T cell responses to bystander allergens or infections (e.g., viruses) (Maizels _et al_, 2018; Zakeri _et al_, 2018). We have previously shown that during chronic schistosomiasis, a pronounced phenotype of activated Tregs in the spleen and lung suppressed ovalbumin-induced allergic airway inflammation (AAI) (Layland _et al_, 2013). Transcriptional profiling of the Tregs revealed upregulation of distinct genes such as _Foxp3, GITR, CD103, OX40, CTLA-4_, and _GrzB_ (Layland _et al_, 2010, 2013). In general, Treg profiles induced by helminth parasites are parasite-specific, that is, heterogeneous. Overall, multiple mechanistic pathways are implicated, involving induction of the cytokines IL-10 and TGF-β (Grainger _et al_, 2010; Maizels _et al_, 2018; Zakeri _et al_, 2018).

1   Institute for Medical Microbiology, Immunology and Hygiene, TUM School of Medicine, Technical University of Munich (TUM), Munich, Germany
2   Center for Global Health, TUM School of Medicine, Technical University of Munich (TUM), Munich, Germany
3   Institute for Immunodeficiency, Center for Chronic Immunodeficiency, Medical Center and Faculty of Medicine, University of Freiburg, Freiburg, Germany
4   Center of Allergy and Environment (ZAUM), Technical University of Munich and Helmholtz Center Munich, Munich, Germany
5   Department of Chemistry, Technical University Munich (TUM), Garching, Germany
6   Department of Neurology, University Hospital, Klinikum rechts der Isar, Technical University Munich (TUM), Munich, Germany
7   Center for Global Health, Institute of Health and Society, University of Oslo, Oslo, Norway
8   Department of Paraclinicals, School of Veterinary Medicine, University of Zambia, Lusaka, Zambia
9   Rheumatology Unit, Department of Medicine, Solna, Karolinska University Hospital, Stockholm, Sweden
10 Center for Pediatrics and Adolescent Medicine, Medical Center, University of Freiburg, Freiburg, Germany
11 Centre for Integrative Biological Signalling Studies, University of Freiburg, Freiburg, Germany
12 German Center for Infection and Research (DZIF), Munich, Germany
    *Corresponding author: Tel: +49 89 4140 4130; E-mail: Clarissa.dacosta@tum.de
    †These authors contributed equally to this work

Infection with the cystic larval stage of the helminth *Taenia solium* causes neurocysticercosis (NCC), a zoonotic inflammatory disease of the CNS in humans and common cause of epileptic seizures worldwide (Winkler, 2012). In NCC, increased levels of Tregs have been reported in both CNS and periphery (Adalid-Peralta *et al*, 2013; Garcia *et al*, 2014a; Prodjinotho *et al*, 2020). Therein, Tregs are believed to limit inflammation in the CNS and in the periphery, but the underlying mechanisms of their induction remain unclear. Treg induction may be mediated by currently unknown cyst products that modulate tolerogenic and hyporesponsive dendritic cells (DCs), which are defined by secretion of immunomodulatory cytokines such as IL-10 and TGF-ß (Adalid-Peralta *et al*, 2013; Arce-Sillas *et al*, 2016; Prodjinotho *et al*, 2020). Recent investigations have associated the presence of the Tregs with asymptomatic NCC, as evidenced by increasingly higher levels of Tregs in cerebrospinal fluid (CSF) and in peripheral circulation of asymptomatic NCC patients, harboring viable cysts, as compared to symptomatic patients with degenerating larval cysts (Adalid-Peralta *et al*, 2013; Arce-Sillas *et al*, 2016; Prodjinotho *et al*, 2020). Thus, the presence of Tregs in NCC seems to be associated with the stage of the larval cyst (viable vs. degenerating). These cells were found to express higher levels of CTLA-4, GITR, and PD-1 in the periphery (Arce-Sillas *et al*, 2016). Nevertheless, the characteristics of these Tregs in the brain and mechanisms regulating their presence (locally induced vs. trafficking from periphery) are currently not known. The progression to symptomatic NCC is usually associated with larval degeneration following natural involution or anthelminthic treatment (Sikasunge *et al*, 2008; Verma *et al*, 2011; Cardenas *et al*, 2014; Mahanty *et al*, 2015; Singh *et al*, 2015).

This progression and ensuing inflammation result in sharp decreases of peripheral and central Treg numbers accompanied by an activation of Iba-1^{high} microglia and higher expression of IL-6, TNFα, IL-17, and TGF-β (Verma *et al*, 2011; Fujita *et al*, 2013; Cardenas *et al*, 2014; Mahanty *et al*, 2015; Singh *et al*, 2015; White *et al*, 2018). The modulation and activation of microglia and DCs by cyst products present in the brain are major components of brain inflammation and neurodegenerative diseases, such as in Toxoplasma infection (Li *et al*, 2019). Following intense inflammation in the CNS that disrupts the integrity of the blood–brain barrier (BBB), various cyst materials can reach the peripheral circulation and can be further distributed in host tissues including lung, liver, muscles (Fleury *et al*, 2016), where they initiate a systemic immune response from macrophages (alveolar macrophages (AM), monocyte-derived (MDM)), and DCs (bone marrow-derived dendritic cell (BMDC)). These cells are main players in the initiation, development, resolution, and chronicization of local inflammation through cytokines and Treg induction, and the modulation of their functions has been show to contribute to inflammation and regulation during NCC (Fleury *et al*, 2016). These observations indicate an important role of Tregs in controlling inflammation in distinct tissues such as CNS. However, the role of different cyst larval stage-driven microglial phenotypic and functional changes in the development of symptomatic NCC or expansion of central Tregs is largely unknown.

Alongside Tregs, the induction of bioactive lipid mediators (LMs), that is, eicosanoids, represents an important immune regulatory mechanism that enables helminths to control inflammation in affected tissues (Esser-von Bieren, 2019; de Los Reyes Jimenez *et al*, 2020; Oyesola *et al*, 2021). LMs, including prostaglandins (PG),

leukotrienes, lipoxins, and thromboxanes, represent a substantial pool of tissue signals that may shape T cell polarization, differentiation, and function, involving resolving inflammation and initiating tissue repair (Esser-von Bieren, 2019). Local production of PGE$_2$ and PGD$_2$ induces DC maturation and the subsequent priming of distinct T cell phenotypes in tissue (Th1 or Th2) (Barrett *et al*, 2011; Kaisar *et al*, 2018). Recently, we found that larval products of the helminth *Heligmosomoides polygyrus bakeri* (HpbE), in particular the enzyme glutamate dehydrogenase (GDH), triggered a switch from 5-lipoxygenase-derived leukotrienes to cyclooxygenase-derived prostanoids abrogating Th2-related AAI (de Los Reyes Jimenez *et al*, 2020). This suppression involved local expression of HIF-1a and a pronounced upregulation of PGE$_2$ and IL-10, and downregulation of cysteinyl leukotrienes in macrophages. In contrast, in NCC, the role of LMs in disease course and outcome has never been evaluated.

In particular, it remained unclear which key immunogenic components derived from the cyst (whole cyst antigenic components, cyst vesicular fluid) regulate classical DC, macrophage, microglia, or lymphocyte function and the influence on eicosanoid pathways with subsequent implications for Treg induction. In this study, using *T. solium* cyst product preparations as models to mimic the *in vivo* situation of viable and degenerating cysts, we found that GDH and isocitrate dehydrogenase (IDH) enzymes present in viable cysts induced a PGE$_2$-IL-10 axis to promote the induction of Tregs. Furthermore, we demonstrated that the inhibition of the IL-10-PGE$_2$ axis in microglia following treatment with degenerating cyst products augmented the expression of TGF-ß, which impaired phagocytosis, and could serve as target to improve NCC. Thus, we have identified important immuno-determinants in the outcome of NCC and revealed targets for therapeutic strategies that may enhance Treg expansion and immune tolerance in inflamed tissues.

Results

Viable cyst products (CLys and CSN) promote the induction of GrzB$^+$ Tregs from naive CD4$^+$ T cells *in vivo* through altering the APC phenotype

An important feature of asymptomatic NCC is a marked increase in CD4$^+$CD25$^+$Foxp3$^+$ Tregs (Adalid-Peralta *et al*, 2012), although the mechanisms of their induction remain largely unknown. In order to investigate this area, we firstly compared the ability of products prepared from viable cysts (cyst lysates (CLys), cyst supernatant (CSN)) and those released into the tissue during treatment-induced or natural death (cyst vesicular fluid (CVF)), to regulate antigen-presenting cell (APC) responses. Thus, we generated BMDCs and AM from C57BL/6 mice and evaluated the induction of TNFα, IL-6, IL-10, and TGF-ß by cyst products (Fig 1A). We observed that while IL-6 was similarly induced by all three materials, CVF had the strongest capacity to induce the release of TNFα from BMDCs and AM. Interestingly however, CVF hardly induced any IL-10 production in contrast to Clys and CSN, both of which induced high levels of IL-10 in BMDCs and AM, and the anti-inflammatory cytokine TGF-ß in AM (Fig 1A). As a consequence, increased TNFα production in the presence of CVF resulted in strong apoptosis and death, especially in AM, whereas both Clys and CSN barely induced BMDC and AM death (Fig EV1A). Interestingly, when analyzing the

morphology of the cells, a significantly greater number displayed a spreading morphology in AM culture treated with CSN than with CVF and Clys (Fig EV1B).

Given the markedly pronounced IL-10 production from BMDCs in presence of Clys and CSN, we hypothesized that this signature may influence BMDC maturation and subsequent functions (e.g., orchestration of Th1, Th2 responses). To this end, we examined whether pre-exposure to Clys and CSN could alter the maturation and response of BMDCs to TLR-ligand LPS stimulation by assessing expression of surface markers, costimulatory molecules, and cytokines, critical for DC functions. We found that BMDCs exposed to Clys and CSN were impaired in the upregulation of MHCII and costimulatory molecules CD86 and CD80 in presence of LPS (Fig 1B), thus acquiring a tolerogenic-like phenotype. In contrast, CVF did not show suppressive effects, but rather fostered the expression of these maturation markers. Accordingly, preincubation with Clys and CSN (but not CVF) resulted in a strongly diminished LPS-induced TNFα and IL-6 response in BMDCs (Fig EV1C).

Since Clys/CSN promoted a tolerogenic-like phenotype in BMDCs and the axis of immature/tolerogenic-like DC-Treg induction is well known in helminth infection (Maizels *et al*, 2018), we next tested whether presence of both products led to an expansion of Tregs *in vitro*. We observed that, unlike CVF, both Clys and CSN were potent in inducing CD4$^+$CD25^{hi}FoxP3$^+$ Tregs after 48–72 h stimulation of spleen cells from C57BL/6 mice (Fig 1C). Next, we assessed the capacity of *in vitro* Clys/CSN-induced tolerogenic BMDCs to induce Tregs *in vivo*. For this, we utilized adoptive transfer of Clys- and CVF-treated and OVA-pulsed-BMDCs into recipient mice, which previously received sorted naïve OT-II CD4$^+$ T cells. Interestingly, mice that received Clys-treated BMDCs had a significant increase in granzyme B-expressing Tregs from naïve OT-II T cells in lymph node in sharp contrast to CVF-treated and OVA-pulsed BMDCs (Fig 1D). Collectively, these results demonstrate that, in contrast to products released during parasite death, viable parasite products licensed a tolerogenic-like phenotype in BMDCs, which promoted suppressive Treg differentiation from naïve CD4$^+$ T cells.

Clys- and CSN-induced Tregs express CNS and the lymphoid homing receptors CCR6 and CCR7

Having shown that only CLys and CSN induced Tregs from naïve murine CD4$^+$ T cells (Figs 1 and EV2A), we next examined this effect in human cells. Thus, using human PBMCs, we observed that, unlike CVF, both CLys and CSN promoted the induction of Tregs characterized as CD4$^+$CD127$^-$CD25^{hi}FoxP3$^+$CTLA-4$^+$ cells (Figs 2A and EV2B). Of note, about 87–90% of the induced CD25^{hi} cells co-expressed FoxP3 and CTLA-4 (Fig 2A). We further noted that the percentage of induced-Tregs in culture markedly increased at day 2, stabilized and subsequently decreased from day 5 (Fig 2A). A critical function for CD4$^+$CD25$^+$CTLA-4$^+$ Tregs is to migrate into the target organs to exert their suppressive action (Sakaguchi *et al*, 2008; Matheu *et al*, 2015). Next, we examined the expression of trafficking receptors CXCR3, CCR4, CCR6, and CCR7 on *in vitro* induced Tregs. CCR6 and CCR7, known to drive the migration of T cells into CNS and secondary lymphoid tissues, were predominantly expressed in presence of both CLys and CSN, which, however, did not affect the expression of CXCR3 and CCR4. Interestingly, CXCR3, CCR6, and CCR4 expression was increased in CD4$^+$CD25$^-$FoxP3$^-$

effector non-Treg cells in contrast to CCR7, which remained unaltered (Fig 2B). The capacity of peripheral Tregs to inhibit T cell activation and proliferation via CTLA-4/IL-10 support their role in controlling (neuro)inflammation (Adalid-Peralta *et al*, 2012). In line with this, we further observed a high expression of IL-10 by CLys- and CSN-induced Tregs, but not of IFNγ, as well as cell proliferation as shown by upregulated Ki67 expression (Fig 2C). Thus, products derived from viable cyst, CLys and CSN, promoted induction of proliferating Tregs, which express classical lymphoid tissue and CNS homing markers.

Treg induction by CLys and CSN is dependent on IL-10 and PGE$_2$ synthesis

We next turned our attention to identifying the specific molecular mechanisms that drive Treg induction *in vitro*. It is well recognized that *in vitro* Treg induction by helminths requires parasite antigens, which induce tolerogenic APCs expressing high levels of anti-inflammatory cytokines such as IL-10 and TGF-β (Adalid-Peralta *et al*, 2012; Lan *et al*, 2012; Nono *et al*, 2012). We first identified the cytokine environment elicited by CVF, CLys, and CSN in PBMCs. We observed that IL-10 and IL-1β were significantly induced in the presence of CLys and CSN in PBMCs culture after 72 h (Fig 3A). Interestingly, whereas IP-10 was exclusively induced by CVF, and CCL2 uniquely by CSN, IL-6 was induced by all products. In contrast, IFNγ, TNFα, IL-4, and IL-17A were hardly detectable. In addition to cytokines, LMs induced by helminth products have recently been shown to regulate T cell responses and, ultimately, maintain immune tolerance through anti-inflammatory actions (Lone & Tasken, 2013; Kaisar *et al*, 2018; de Los Reyes Jimenez *et al*, 2020). Up to now, however, no link to Treg induction has been established. Indeed, we found induction of bioactive LMs in the presence of all helminth products in PBMCs via LC-MS/MS-based profiling of culture supernatants. Yet, only CLys and CSN significantly stimulated release of the prostaglandins PGE$_2$ and PGD$_2$ after 24 h (Fig 3B). Moreover, CLys and CSN led to a marked increase of TXB$_2$ and LTB$_4$ but a strong reduction in the generation of LXA4, 15-HEPE, and 12, 13-DiHOME. The latter, however, was increased only in the presence of CVF. Interestingly, whereas CLys potently induced the LMs 5-HETE, 11-HETE, 12-HETE, 5-HEPE, and 12-HEPE, CSN failed to do so. Importantly, the bioactive LMs were detected only in culture supernatants, but not within the cyst products, indicating that they were host cell-derived (Fig 3B).

IL-10 and PGE$_2$ were concomitantly induced by CLys and CSN, and PGE$_2$ levels in culture positively correlated with Treg induction (Fig 3C). Since both have been associated with immune suppression in inflammatory diseases and allergy (Betz & Fox, 1991; de Los Reyes Jimenez *et al*, 2020), we next sought to investigate their implication in Treg induction. Therefore, we performed a simultaneous inhibition of the two major receptors of PGE$_2$ involved in immune modulation, EP2 and EP4, in combination with an IL-10R antagonist. We found that, whereas blocking IL-10R resulted almost in no reduction in Treg inhibition, inhibition of EP2/EP4 attenuated the induction of Treg by both CLys and CSN (Fig EV3A). Similarly, using mPGES1 inhibitor abrogated Treg induction (Fig 3D) confirming the implication of PGE$_2$. Strikingly, blocking both PGE$_2$ and IL-10 resulted in a significantly lower percentage of Treg. To provide
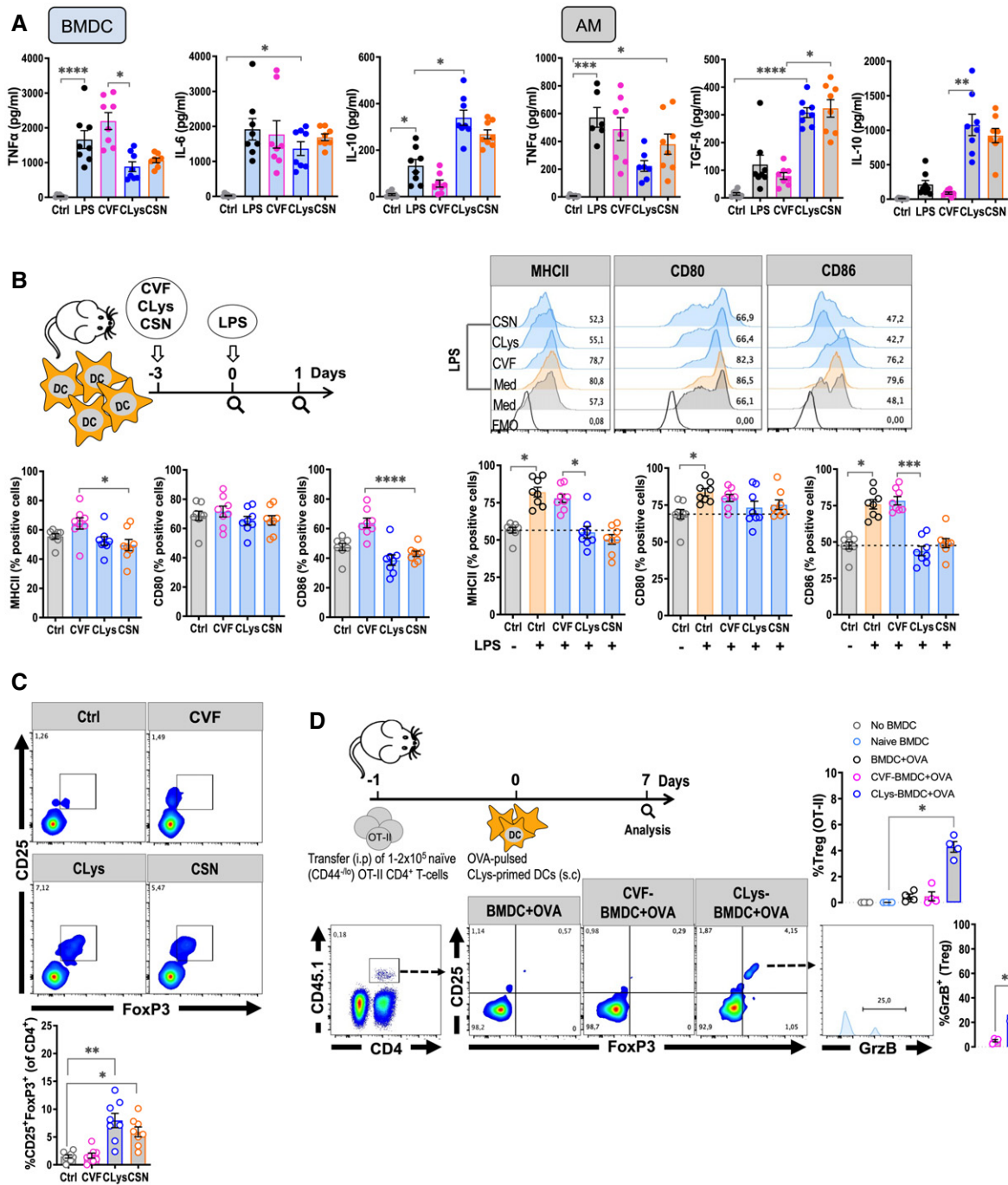
Figure 1. CLys and CSN, in contrast to CVF, promote tolerogenic-like phenotypes of BMDCs resulting in *in vivo* expansion of GrzB$^+$ Tregs.

A   Cytokine levels (TNFα (24 h), IL-6, TGF-ß, and IL-10 (72 h)) in supernatants collected from BMDC and AM culture in presence or not (Ctrl) of LPS (50 ng/ml), CVF, CLys, and CSN (10 μg/ml).

B   FACS assessment of BMDC maturation pre-exposed or not (Med Ctrl) to CVF, CLys, and CSN for 72 h (left panel) before stimulation with LPS for 24 h (right panel). A representative histogram of each condition is shown.

C   Induction of Tregs (CD4$^+$CD25^{hi}FoxP3$^+$ cells) from spleen cells incubated with CVF, CLys, and CSN for 72 h.

D   Induction of Tregs *in vivo* after adoptive transfer of BMDCs pretreated for 48 h with CVF or CLys and pulsed for 24 h with OVA (20 μg/ml) into recipient mice, which had received sorted naïve CD45.1-OT-II cells. On day 7, the lymph nodes were collected and end points analysis was performed.

Data information: Graphs are representative of 8 biological replicates (*n* = 8) (BMDCs, AM, spleen cells) for (A-C) and 4 biological replicates (*n* = 4) for (D). For (B), populations were pre-gated on CD11c$^+$. Results are expressed as means ± SEM. Asterisks show significant statistical differences analyzed using Kruskal–Wallis one-way ANOVA followed by a Dunn's multiple comparison test. *P < 0.05; **P < 0.01; ***P < 0.001; ****P < 0.0001.
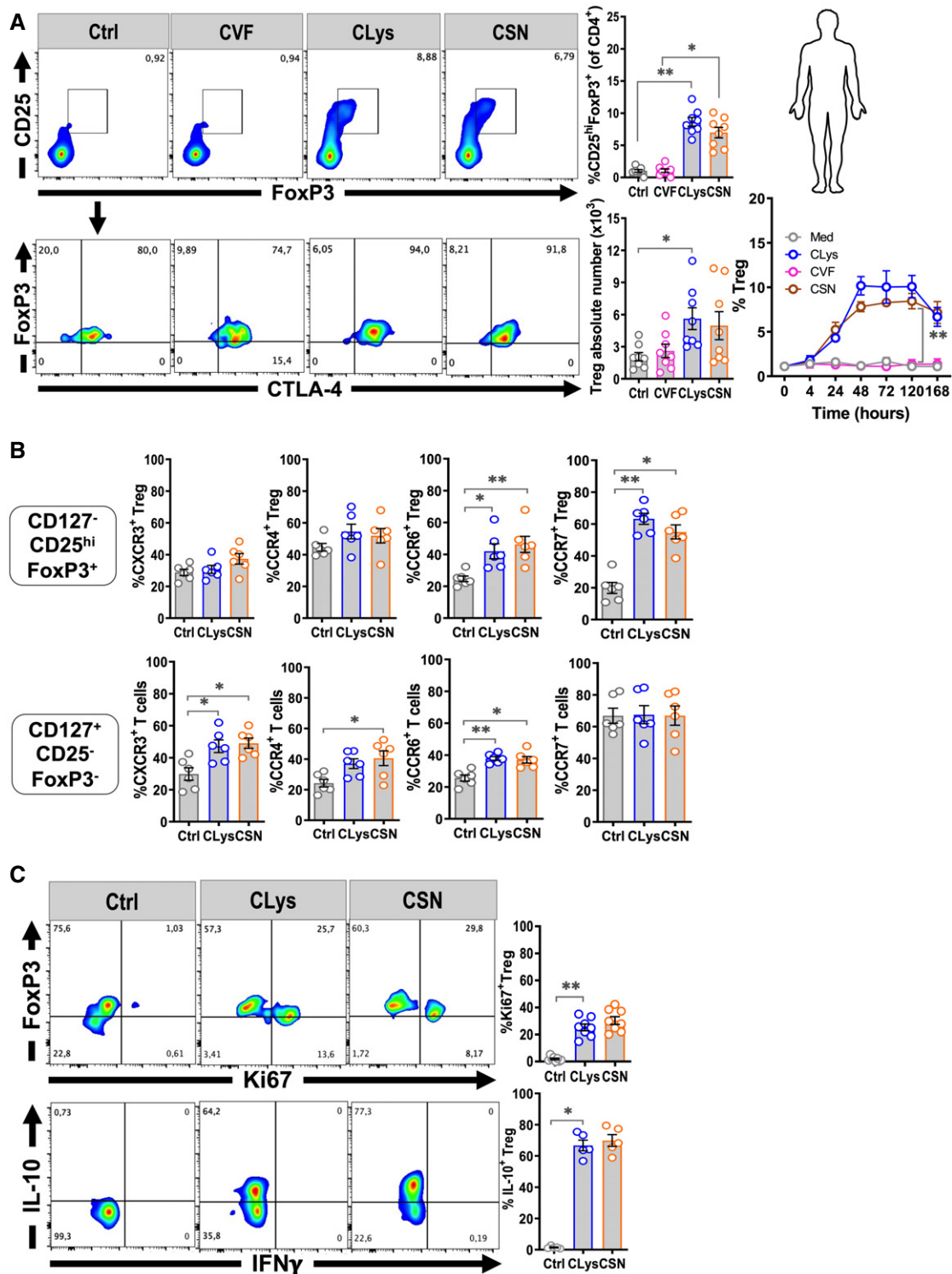
Figure 2. CLys- and CSN-induced Tregs with CNS and lymphoid tissues homing capacity.

A CD4+CD127−CD25hiFoxP3+CTLA4+ Treg induction from PBMCs incubated with CVF, CLys, and CSN (10 μg/ml) after 4, 24, 48, 72 h (plots and graphs shown), 120 h, and 168 h.

B Trafficking receptors (CXCR3, CCR4, CCR6, and CCR7) evaluation on induced Treg (CD25hiCD127−) and non-Treg cells (CD127+CD25−).

C Induced Treg proliferation with Ki67 staining and Treg expression of IL-10 and IFNγ.

Data information: For (C), populations were pre-gated on CD4+CD127−CD25hi. Graphs are representative of 6–8 biological replicates (n = 6–8) for (A-B) and 5–8 biological replicates (n = 5–8) for (C). Results are expressed as means ± SEM. Asterisks show significant statistical differences analyzed using Kruskal–Wallis one-way ANOVA followed by a Dunn's multiple comparison test. *P < 0.05; **P < 0.01.
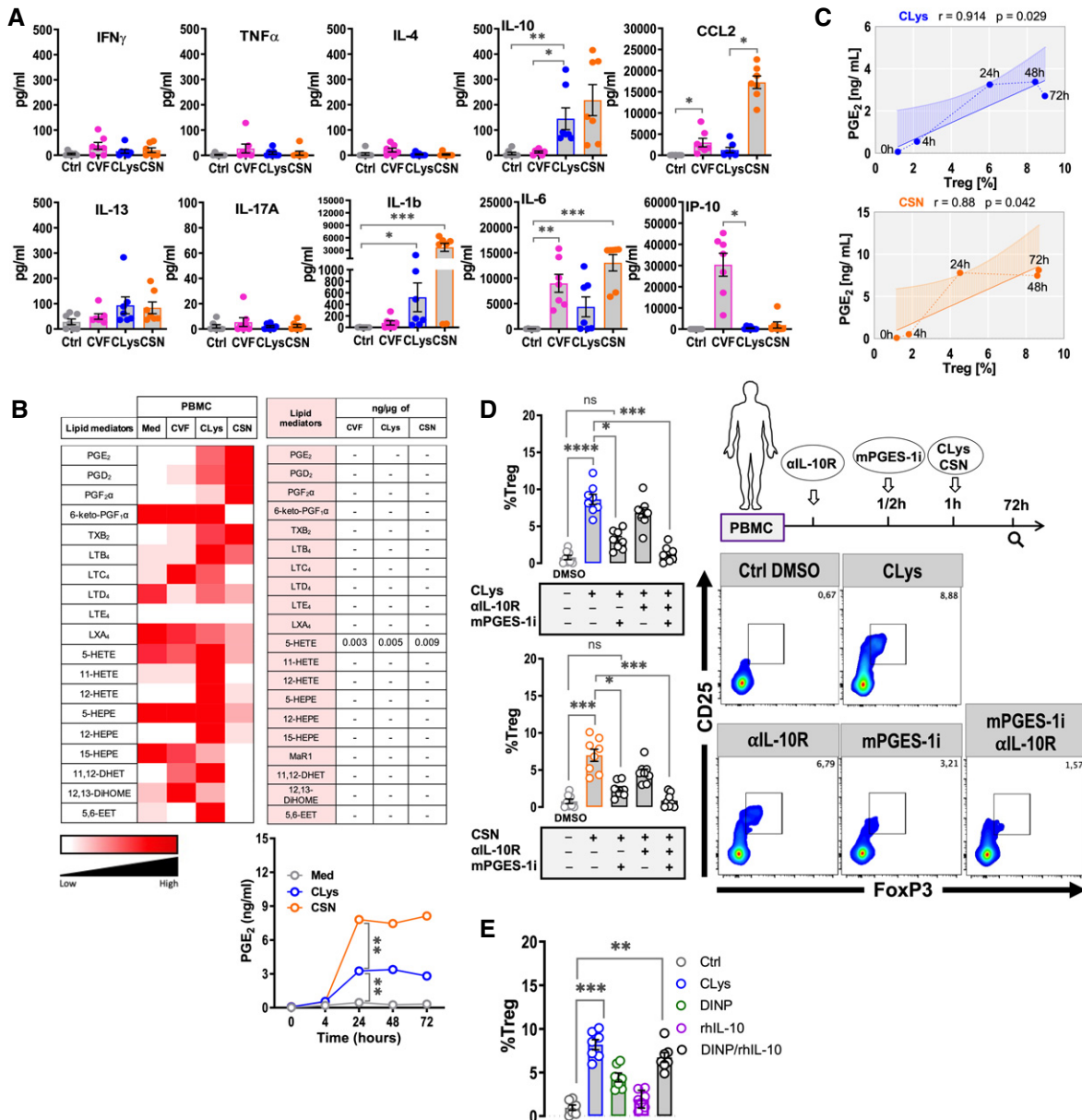
Figure 3. Treg induction by CLys and CSN is PGE$_2$- and IL-10-dependent.

A Levels of pro- and anti-inflammatory cytokines in PBMC culture supernatants with CVF, CLys, and CSN (10 μg/ml) after 72 h determined using a LUMINEX-based technology.

B Composition and levels of bioactive lipid mediators (LMs), including prostaglandins, leukotrienes, lipoxins, thromboxanes, and their precursors in culture with CVF, CLys, and CSN quantified by LC-MS/MS-based profiling. Heat maps show relative amounts of LMs detected by LC-MS/MS in supernatants. Asterisks show statistical differences analyzed using two-way ANOVA followed by Turkey's multiple comparison test.

C Dynamic of PGE$_2$ release correlated with Treg induction by CLys (upper panel) and CSN (lower panel) using a Pearson correlation.

D Treg induction by CLys or CSN following PBMC preincubation with 10 μM mPGES1 inhibitor 934 (or DMSO as a control).

E Induction of Tregs with PGE$_2$ analog (DINP) (5 μM) and/or recombinant human IL-10 (rhIL-10) (10 ng/ml) as compared to CLys.

Data information: Graphs are representative of 7–8 biological replicates (n = 7–8). Results are expressed as means ± SEM. Asterisks show significant statistical differences analyzed using Kruskal–Wallis one-way ANOVA followed by a Dunn's multiple comparison test. *P < 0.05; **P < 0.01; ***P < 0.001; ****P < 0.0001.

additional mechanistic insights, we inhibited TGF-β, regularly associated with Treg expansion in helminth infection, and observed an even further decreased Treg induction (Fig EV3A). Finally, incubation of PBMCs with the PGE$_2$ analog dinoprostone (DINP) in combination with rhIL-10 significantly promoted the development of Tregs in culture (Figs 3E and EV3B). Cumulatively, these findings demonstrate that CLys and CSN derived from viable parasite induce Treg via IL-10 and PGE$_2$ derived from PBMCs.

CLys and CSN mediate Treg induction from naïve CD4$^+$ T cells by sensing PGE$_2$ and IL-10 secretion in tolerogenic-like monocytes

Next, we explored the cellular source of the Treg-driving mediators PGE$_2$ and IL-10. In peripheral blood, monocytes are known to be an important source of LMs (James *et al*, 2001; Sokolowska *et al*, 2014; Sorgi *et al*, 2017). To test the role of monocytes in the production of PGE$_2$ and other LMs in PBMC, we isolated monocytes (Mo^{pos}) from peripheral blood and separated the monocyte-negative fraction (Mo^{neg}) (Figs 4A and EV4). Both Mo^{pos} and Mo^{neg} were incubated with CVF, CLys, and CSN for 72 h and the levels of bioactive LMs in supernatant quantified. We confirmed that LMs were mainly released by monocytes (Fig 4A, left panel) and their expression profile was comparable to that in PBMC. In line with this, IL-10 induction by CLys and CSN was markedly associated with monocytes (Fig 4A, right panel). Having identified monocytes as the major producers of PGE$_2$ and IL-10, which in our settings induced Treg, we further sought to confirm these cells to be instrumental in the induction of Tregs. Indeed, the absence of monocytes significantly decreased the Treg proportion in culture with both CLys and CSN (Fig 4B, left panel). Similar results were observed in the presence of monocytes when the effect of PGE$_2$ and IL-10 was blocked. To identify the mechanistic pathway in greater detail, we inhibited PGE$_2$ receptors either on Mo^{pos} or Mo^{neg} before coculture in presence of CSN. Blockade of PGE$_2$/IL-10 effects on Mo^{neg} significantly suppressed Treg induction by CSN (Fig 4B, right panel), and to a lesser extent on Mo^{pos}, indicating that PGE$_2$/IL-10 axis works efficiently in a paracrine fashion. To further clarify from which cell compartment in Mo^{neg} Tregs are induced (conversion from naïve T cells or expansion of pre-existing Treg cells), we purified naïve CD4$^+$CD45RA$^+$CD45RO$^-$ T cells and demonstrated that most of the induced Tregs (> 95%) in culture are converted from naïve CD4$^+$ T cells (Fig 4C). Subsequently, the analysis of purified monocyte phenotype showed that these cells acquired an M2-like profile in the presence of both CLys and CSN by upregulating the expression of the mannose receptor CD206 and the scavenger receptor CD163 (Fig 4D). In contrast, CVF stimulated a significant increase in the pro-inflammatory (M1) markers CD68 and CD80 on monocytes.

Upon activation, monocytes extravasate from the bloodstream into tissues where they replenish the pool of tissue-resident macrophages. To investigate the helminth product effects on macrophages, we assessed the LMs profile in the supernatant of differentiated macrophages from monocytes (MDM) stimulated with the three products (Fig 4E). Overall, LM profiles were comparable to that of monocytes confirming the capacity of CLys and CSN to induce LMs in macrophages. Interestingly however, MDM produced less PGE$_2$ and no PGD$_2$ and PGF$_2\alpha$ in the presence of CLys in contrast to CSN. Consistent with higher levels of the prostaglandins PGE$_2$, PGD$_2$, and PGF$_2\alpha$ after treatment with CSN, we detected elevated gene expression levels of the enzymes *PTGES* and *PTGS2*. In contrast, the expressions of *MaR1* and the enzymes *ALOX5* and *ALOX15*, which are involved in the generation of leukotrienes and lipoxins (LTB$_4$, LTC$_4$, LTD$_4$, LTE$_4$ and LXA$_4$), were down-regulated. Indeed, these were not detectable in CSN-treated MDM (Fig 4E). In addition, conditioning monocytes with CLys and CSN resulted in significant Treg induction from naïve CD4$^+$ T cells in presence of culture supernatant (Fig 4F).

We conclude from these results that monocytes and macrophages respond to CLys and CSN by upregulating the production of IL-10 and PGE$_2$, which contribute to Treg induction.

GDH and IDH derived from CLys and CSN are the main inducers of Tregs via PGE$_2$ and IL-10

We next sought to identify the active molecules in both CLys and CSN that sensitized monocytes for Treg induction. To this end, we first treated CLys and CSN with proteinase K (PK) and evaluated their ability to induce Treg from PBMC. Notably, our results showed that the Treg induction capacity of both CLys and CSN was strongly decreased after proteinase K treatment (Fig 5A), indicating that active Treg inducers, most likely, consist at least in part of proteins. Next, we evaluated global protein signatures by mass spectrometry in CLys and CSN and, subsequently, screened the reported biological functions of the relatively abundant detected overlapped molecules in CLys and CSN against PGE$_2$ and IL-10. We identified 425 proteins commonly distributed in CLys and CSN (Fig 5B and Dataset EV1). Of those, GDH and IDH, with relatively high scores, have been recently postulated to induce PGE$_2$ and IL-10 and to be involved in *de novo* production of LMs (Badur *et al*, 2018; de Los Reyes Jimenez *et al*, 2020). Thus, we pretreated PBMCs with GDH and IDH inhibitors (bithionol (BT) and IDH-305), alone or in combination, to block activity and downstream signaling of GDH and IDH, before incubation with CLys and CSN. Remarkably, although there was a decrease after IDH-305 treatment, only pretreatment with bithionol alone or in combination with IDH-305 significantly abrogated Treg induction in culture (Fig 5C). In line with the reduced Treg induction, the release of IL-10 and PGE$_2$ from PBMCs was similarly impaired after pretreatment with both inhibitors without affecting cell viability (Fig 5C). As pretreatment with bithionol alone significantly abrogated Treg induction, we, then, investigated the implication of *T. solium* GDH (TsGDH). We successfully purified recombinant (r)TsGDH from an *E. coli* expression system and tested whether TsGDH can recapitulate the effects of CLys/CSN in our settings. We observed a significant induction of Treg in presence of 5 µg/ml of rTsGDH (Fig 5D) via conversion of naïve CD4 T cells (Fig 5E). This correlated with marked PGE$_2$ and IL-10 in the culture supernatants of monocyte-CD4 and monocyte alone (Fig 5D and E). Finally, to rule out any role of endogenous cellular GDH, we tested recombinant human GDH (rhGDH) expressed in *E.coli* and could not observe any Treg induction (Fig 5F), suggesting a specific effect of TsGDH. These observations provide strong evidence for the central role of GDH and IDH within CLys and CSN in Treg induction *in vitro*, suggesting a conserved role of helminthic GDH enzymes in immune regulation (de Los Reyes Jimenez *et al*, 2020).

CLys and CSN regulate PGE$_2$ and IL-10 secretion and phagocytosis in microglia resulting in Treg induction

Microglia, the main resident macrophage population and primary innate immune cells of the brain, maintain brain homeostasis and regulate local immune responses. As such, effective activation/regulation of their phenotype, phagocytic capacity, and trophic factors (e.g., TGF-ß) as well as cytokine production (e.g., IL-10) is crucial for regulating CNS inflammation, which contributes to neuropathological manifestations such as epilepsy, a hallmark in NCC
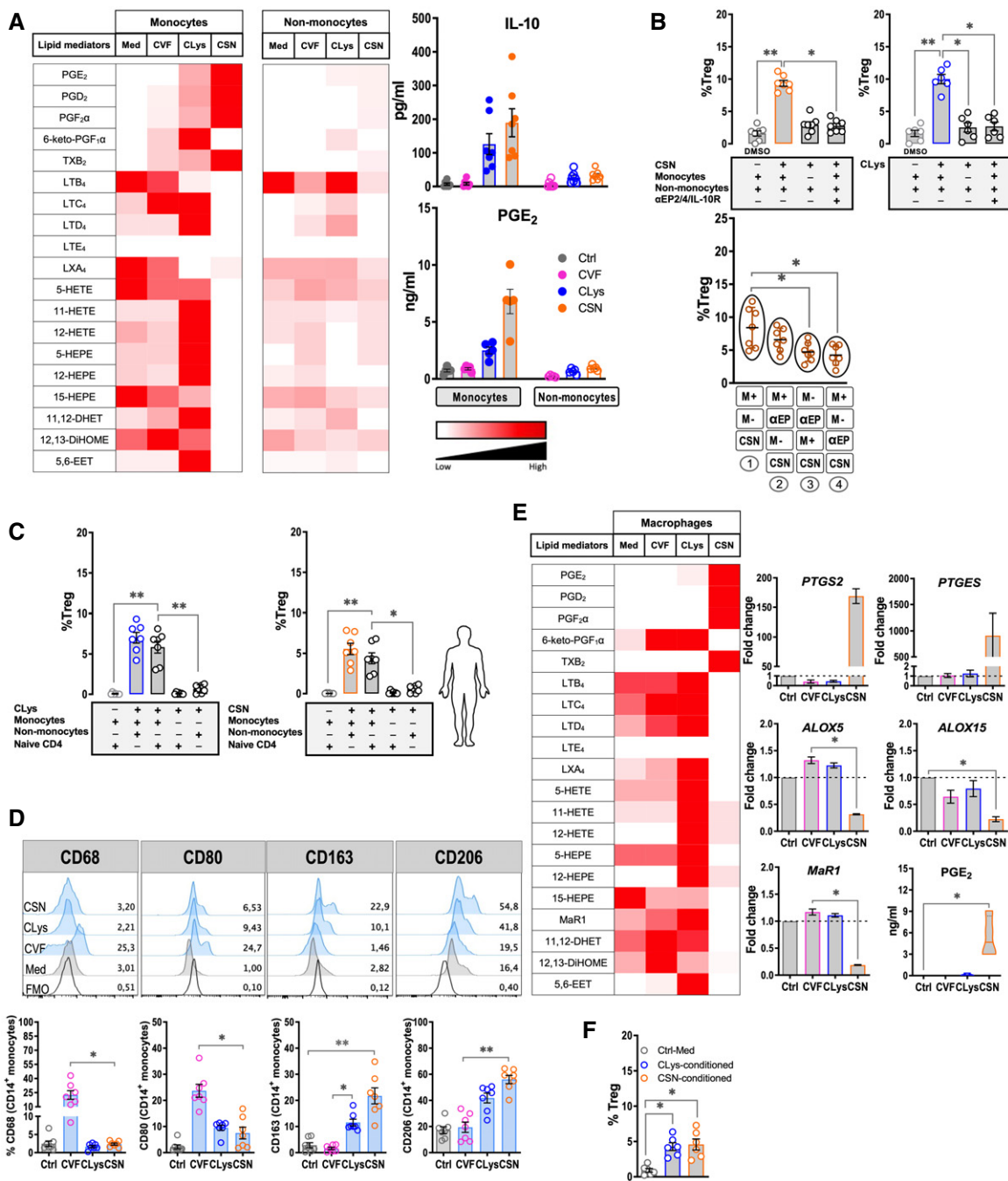
Figure 4. CLys and CSN mediate Treg induction from naïve CD4^{+}T cells via PGE$_2$ and IL-10 secretion from monocytes.

A   Levels of bioactive LMs and IL-10 released from monocyte and non-monocyte fractions.

B   Non-monocyte fractions were preincubated with IL-10R inhibitor and PGE$_2$ receptor (EP$_2$ and EP$_4$) antagonists (or DMSO as a control) and incubated with CLys (left upper panel) or CSN (10 μg/ml) (left lower panel) in presence or absence of monocytes and Treg induction was analyzed after 72 h. On the right panel, PGE$_2$ receptors were first blocked on monocytes (2) or non-monocytes (3) or both (4) before addition of non-monocytes (2) or monocytes (3) and incubation with CSN for 72 h and analysis of Treg induction compared to control condition (1).

C   Treg induction by CLys and CSN in presence of monocyte/non-monocyte fractions and naïve CD4^{+}CD45RA^{+}CD45RO^{−} T cells.

D   Monocyte phenotyping in presence of CVF, CLys, and CSN by FACS using CD68, CD80, CD163, and CD206 surface expression.

E   Levels of LMs and PGE$_2$ released by macrophages in presence of CVF, CLys, and CSN Additionally, macrophages were lysed and gene expression of *PTGS2*, *PTGES*, *ALOX5*, *ALOX15*, and *MaR1* quantified by RT–PCR.

F   Treg induction following naïve CD4^{+}CD45RA^{+}CD45RO^{−} T cells incubation with CLys- and CSN-monocyte conditioned media.

Data information: Heat maps in (A) and (D) show relative amounts of LMs detected by LC-MS/MS in supernatants. Data and graphs are representative of 6–7 biological replicates (n = 6–7) for (A, B, C, D, F) and 4 biological replicates (n = 4) for (E). Results are expressed as means ± SEM. Asterisks show significant statistical differences analyzed using Kruskal–Wallis one-way ANOVA followed by a Dunn's multiple comparison test. *P < 0.05; **P < 0.01.
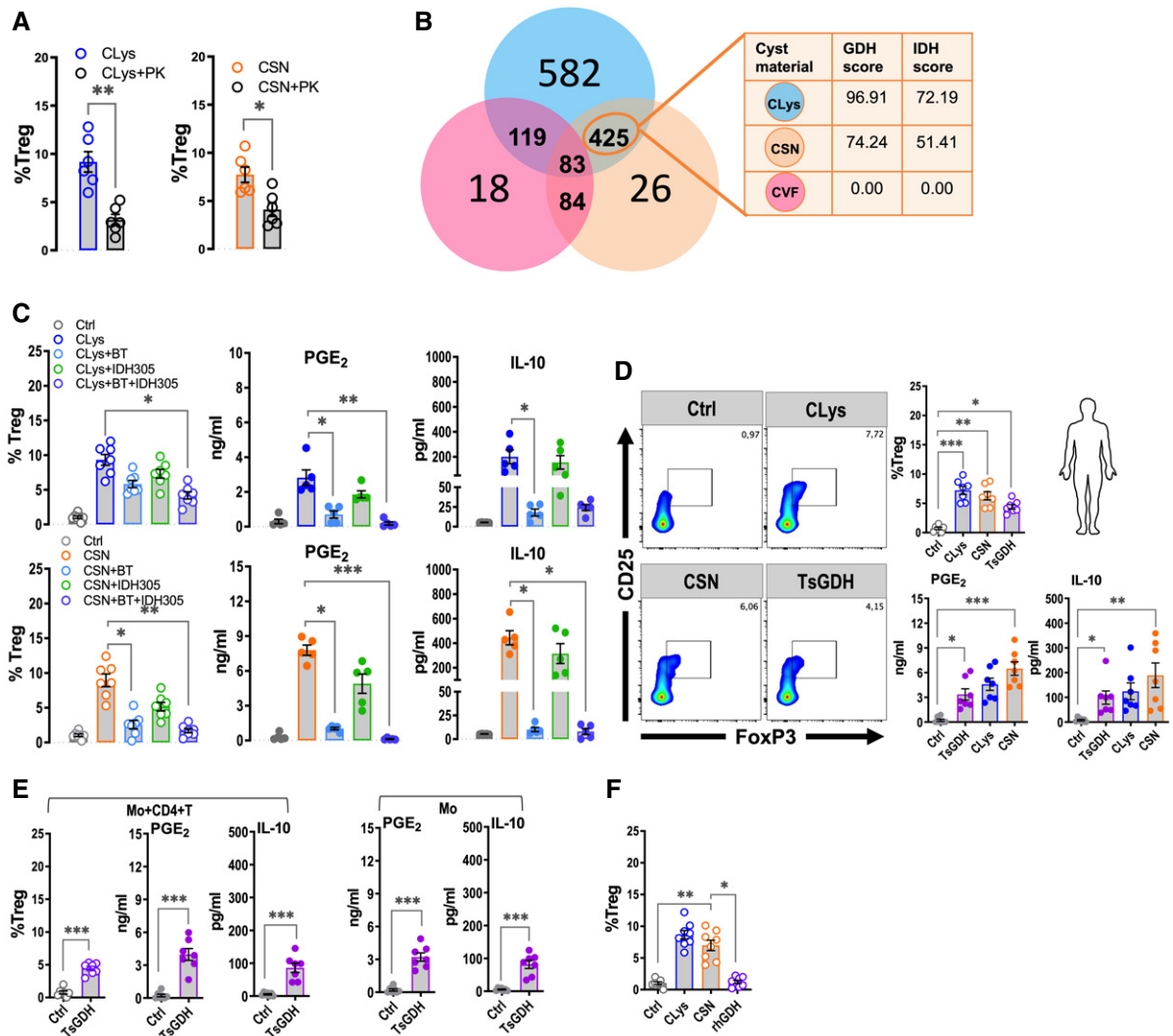
Figure 5. *Taenia solium* GDH and IDH license Treg induction from naïve CD4^{+} T cells via PGE$_2$ and IL-10 secretion.

A   Induction of Treg following PBMC treatment with either native or proteinase K-treated CLys or CSN (10 μg/ml) for 72 h.
B   Mass spectrometry analysis of CVF, CLys, and CSN and identification of distinct and shared proteins. From the shared proteins in CLys and CSN, relative detection scores of GDH and IDH were presented.
C   PBMCs were treated with GDH inhibitor bithionol (BT) (20 μM) or IDH inhibitor IDH-305 (50 nM) alone or in combination before incubation with CLys or CSN. Percentage of Treg was determined and PGE$_2$ and IL-10 levels were evaluated.
D   Treg induction from PBMC by CLys, CSN, and TsGDH (5 μg/ml) and levels of PGE$_2$ and IL-10 in culture supernatants.
E   Treg induction from monocyte-naïve CD4^{+}-TsGDH culture and levels of PGE$_2$ and IL-10 in monocyte-CD4^{+}-TsGDH and monocyte-TsGDH culture supernatants.
F   Treg induction from PBMC by CLys, CSN, and rhGDH (10 μg/ml).

Data information: Graphs are representative of 5–7 biological replicates (n = 5–7) for (A-E) and 8 biological replicates (n = 8) for (F). Results are expressed as means ± SEM. Asterisks show significant statistical differences analyzed using Mann–Whitney U test (A) or Kruskal–Wallis one-way ANOVA followed by a Dunn's multiple comparison test (C). *$P < 0.05$; **$P < 0.01$; ***$P < 0.001$.

(Devinsky *et al*, 2018; Carmen-Orozco *et al*, 2019). Having demonstrated that CLys and CSN induced PGE$_2$ and IL-10 in monocytes and macrophages, which potentiated Treg induction, we interrogated whether this effect would be reflected by microglia. First, we examined the expression of MHCII and Iba-1 as markers of microglia activation/reactivity *ex vivo* (Fig 6A). Microglia displayed a low basal level expression of MHCII/Iba-1 under control conditions, which increased in the presence of all cyst products (Fig 6A).

Nonetheless, CVF led to higher expression of these activation markers compared to CLys and CSN, although this difference was not statistically significant.

Next, we investigated how the different products would affect microglia function. RT–PCR was then employed to determine the relative expression levels of inflammatory and regulatory mediators, important upstream of microglia function. We observed that CLys and CSN treatment of microglia significantly upregulated the
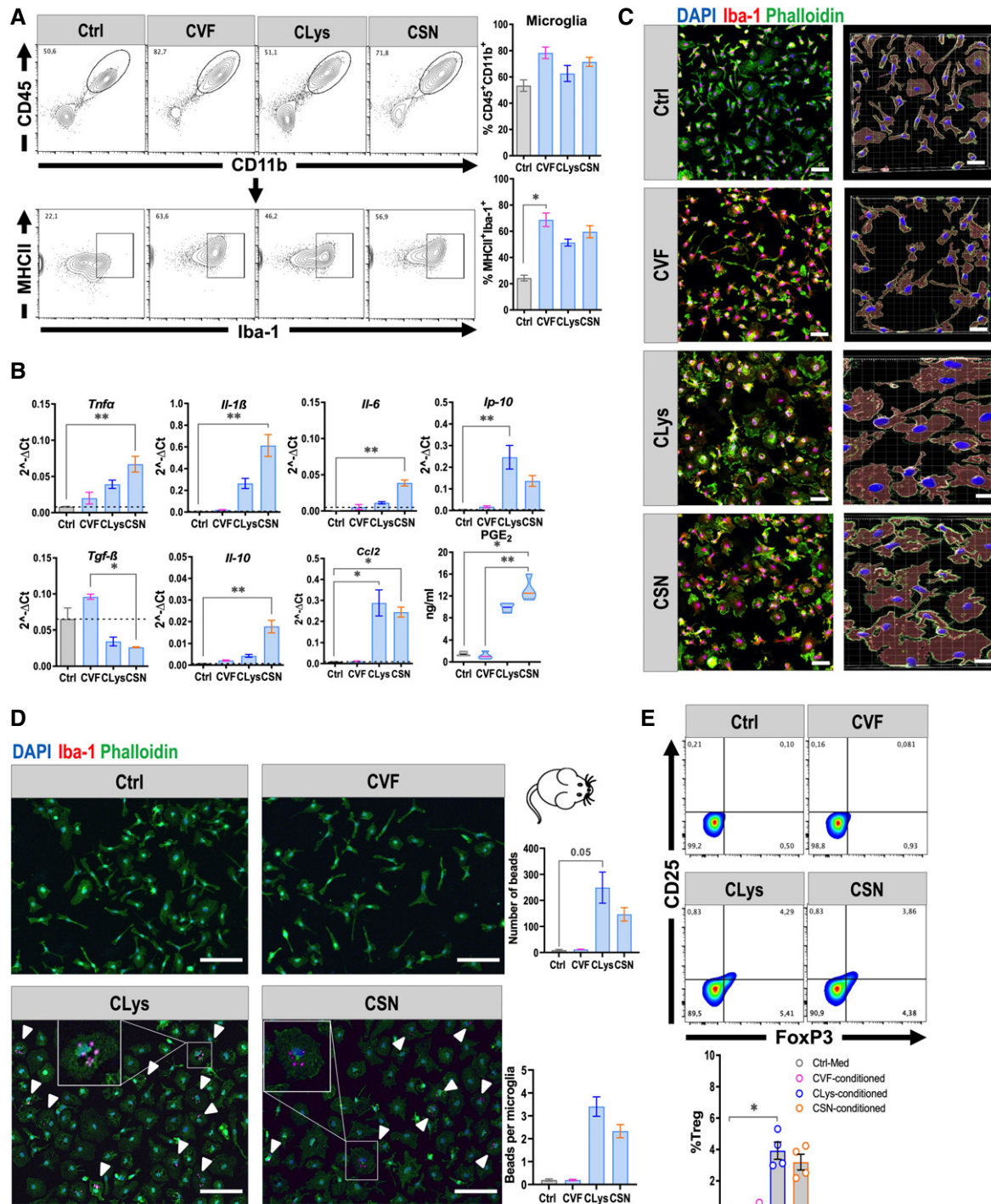
Figure 6. Induction of PGE$_2$ and IL-10 by CLys and CSN is associated with phagocytosis in microglia and Treg induction.

A Phenotype and activation of newborn microglia in presence of CVF, CLys, and CSN (10 μg/ml).

B RT–PCR for pro- and anti-inflammatory genes from microglia and culture supernatant levels of PGE$_2$.

C Confocal microscopy immunofluorescence of Iba-1 staining (left panel) and 3D microglia morphology and shape in presence of CVF, CLys, and CSN. Scale bar (50 μm) applies to all images.

D Red-fluorescent latex bead uptake by CVF-, CLys-, and CSN-stimulated microglia by confocal microscopy and total number of bead uptake per microglia. Arrowheads show bead uptake by single microglia. Scale bar (100 μm) applies to all images.

E Treg induction following naïve CD4$^+$CD62L$^+$ T cells incubation with CVF-, CLys-, CSN-microglia conditioned media.

Data information: Graphs are representative of 4 biological replicates ($n = 4$). Results are expressed as means ± SEM. Asterisks show significant statistical differences analyzed using Kruskal–Wallis one-way ANOVA followed by a Dunn's multiple comparison test. *$P < 0.05$; **$P < 0.01$.

expression of *Il-1β*, *Il-6, Ip-10*, and *Ccl2* (Fig 6B). Interestingly, whereas all products increased the expression of *TNFα*, the neurotrophic TGF-ß was uniquely induced by CVF. Importantly, microglia stimulated with CLys and CSN exhibited a significant upregulation of *Il-10* and formation of PGE$_2$ in microglia similar to the situation of peripheral monocytes (Fig 6B) and macrophages. We further performed immunofluorescence microscopy and confirmed increased Iba-1 expression in presence of CVF (Fig 6C, left panel). Furthermore, when analyzing the microglia morphology, we found that CLys and CSN induced a similar large ameboid morphology (Fig 6C, right panel). In contrast, CVF induced a more elongated, branched, and ramified shape, which is commonly associated with a nonphagocytic phenotype in microglia (Aloisi, 2001; Lan *et al*, 2017). This led us to address the phagocytic activity of microglia in

presence of CVF, CLys, and CSN. In line with the elongated and branched shape, CVF-stimulated microglia were impaired in their phagocytic activity (Fig 6D). In comparison, there was a significant uptake of latex beads by microglia (2,5–4 per microglia) in culture with CLys and CSN (Fig 6D). Finally, we demonstrated that culture media harvested from microglia conditioned in the presence of CLys and CSN, in contrast to CVF, actively promoted Treg differentiation from naïve CD4$^+$ CD62L$^+$ T cells (Fig 6E) confirming previous data (Fig 4B) demonstrating the requirement of monocytes in inducing Treg. Thus, CLys and CSN potentiated IL-10 and PGE$_2$ release from microglia associated with a less inflammatory and higher phagocytic activity and the capacity to induce Treg differentiation. A proposed model of *T. solium* cyst stage-driven immune modulation and signaling in CNS (Fig 7A) and in periphery (Fig 7B) is presented in Fig 7.
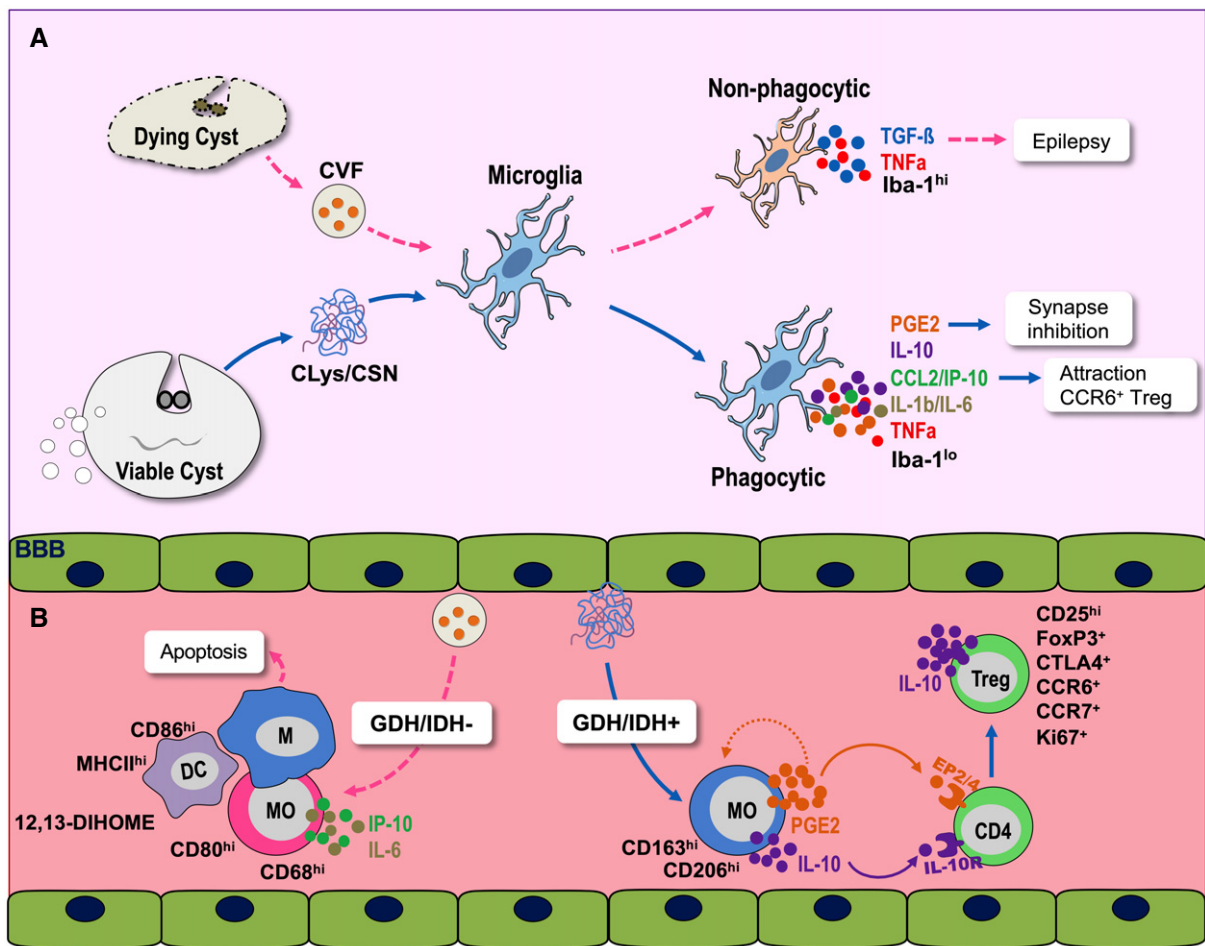

Figure 7. Proposed model of CVF-, CLys/CSN-driven cell modulation and signaling in the periphery and in the CNS.

A   In CNS, viable cyst antigen and excretory-secretory products (CLys/CSN) promote a phagocytic phenotype from resident brain microglia expressing low Iba-1 but high CCL2, IP-10, IL-10, and PGE$_2$, a potential synaptic inhibitor. After cyst degenerates, dead cyst materials and released vesicular fluid (CVF) interact with microglia and polarize an inflammatory and nonphagocytic phenotype with high expression of Iba-1 and the pro-epileptic TGF-ß.

B   In periphery, GDH/IDH from CLys/CSN license tolerogenic CD163^{hi}CD206^{hi} monocytes to express IL-10 and PGE2, which can then bind to IL-10R and EP2 and EP4 on CD4$^+$ T cells driving the expansion of CD25^{hi}FoxP3$^+$CTLA4$^+$ Tregs expressing IL-10 and the CNS homing receptors CCR6 and CCR7. When dead cyst products (CVF) reach the periphery, not yet identified active molecule promotes an inflammatory phenotype in monocyte and mature dendritic cells with high expression of CD68, CD80, CD86, and MHCII, while selectively inducing apoptosis in macrophages associated with significant synthesis of TNFα and the eicosanoid 12,13-DIHOME. DC, dendritic cell; GDH, Glutamate dehydrogenase; IDH, Isocitrate dehydrogenase; M, macrophage; M0, monocyte.

Discussion

In this study, we describe a key role of PGE_2 in promoting Treg differentiation from tolerogenic APCs in the context of helminth-mediated immune regulation. We found that products derived from viable *T. solium* cysts (CLys and CSN), in contrast to dead cyst-derived products (CVF), promoted tolerogenic monocytes, dendritic cells, and macrophages with an increased capacity to induce Tregs. During LPS-induced inflammation, viable cyst products repressed the expression of MHCII and of the costimulatory molecules CD80 and CD86 as previously demonstrated for another helminth parasite (Nono *et al*, 2012). The adoptive transfer of tolerogenic (CLys/CSN-treated) murine BMDCs potentiated the differentiation of local Tregs from naïve $CD4^+$ T cells in an OVA-specific fashion, which was absent in mice that received CVF-pre-treated BMDCs. This suppressive activity was further confirmed in CLys/CSN-conditioned human PBMC in which CTLA-4 and IL-10 was significantly upregulated in induced Treg. In contrast, symptomatic NCC could be the consequence of decaying cysts, due to the strong capacity of intravesicular products (CVF) to induce TNFα from peripheral APCs (DCs and macrophages). We thus can add to the previously shown capacity of whole cysts to induce Tregs (7) that this capacity requires viable cysts as well as the products they secrete and does not emanate from CVF, which is potentially released by degenerating cysts. Indeed, CVF appears to behave in a rather pro-inflammatory manner by triggering the release of TNFα rather than immunoregulatory TGF-ß and IL-10 from APCs.

IL-10 is not only a suppressive cytokine but has also been recognized to mediate Treg polarization in previous studies showing important immune regulatory roles of TGF-β or TGF-β-like molecules from helminth parasites (Grainger *et al*, 2010; Arce-Sillas *et al*, 2016). We demonstrated in our setting that IL-10 in combination with PGE_2, rather than TGF-β, licensed Treg induction from PBMCs *in vitro*. PGE_2 represents one of the most abundant prostaglandins in tissue and as such is a promising biological target (Dennis & Norris, 2015). The induction and function of PGE_2 and IL-10 are controlled by antigen-, context- and tissue-specific modalities (Dennis & Norris, 2015). Using *T. solium* viable larval products, we have uncovered a new function of PGE_2 in inducing Tregs in the context of helminth infections. We found that PGE_2 induced $CD4^+CD25^+FoxP3^+CTLA-4^+$ Treg cells through the receptors EP2 and EP4, which have been previously shown to trigger anti-inflammatory signals in T cells through protein kinase A (PKA)-cAMP signaling (McCullough *et al*, 2004; Boniface *et al*, 2009), which should thus be investigated as a potential upstream mechanism underlying the induction of Treg by CLys and CSN in our setting. Indeed, the expression and role of PGE_2 receptors EP2/4 and, thus, the regulation of cell behavior and immunological effects of PGE_2 (e.g., Treg induction) are complex and context-dependent (disease, tissue, co-signal). For instance, while PGE_2 has the potential to support Treg expansion by TGF-ß-Smad2/3 signaling (English *et al*, 2009; Cho *et al*, 2015), it has also been shown to inhibit this signal via stimulation of ERK1/2, PI3K/AKT, and 3'5'-cAMP phosphorylation, which degrade Smad2/3 signaling (Thomas *et al*, 2007; Goepp *et al*, 2021). Whereas our settings suggest that induction of PGE_2 may contribute to a mechanism by which parasitic worms induce Tregs to control host immune attack, it may inhibit unwanted suppressive Treg activity in distinct immunological

settings and tissue environments (e.g., tumor environment, intestine). Moreover, the canonic functions of EP2 and EP4 can switch in specific tissues and cell types. Recently, endogenous PGE_2 has been demonstrated to down-regulate intestinal Treg accumulation and responses by affecting the composition of the gut microbiota and modulating the function of mononuclear phagocytes in mice (Crittenden *et al*, 2021). However, this effect is less potent in mLN and spleen (Crittenden *et al*, 2021). Of note, EP2 expression is pronounced on peripheral blood T cells in contrast to colonic T cells presenting higher EP4 expression (Harris *et al*, 2002). Finally, the suppressive effect of PGE_2 on immune cells is affected by TCR-signaling. Thus, PGE_2 inhibited Treg conversion via EP2 and EP4 in co-stimulation of murine splenic, colonic, and peripheral blood human naïve T cells with TGF-ß in presence of TCR activators (αCD3/αCD28) and/or cytokines (IL-2, IL-12) (Narumiya *et al*, 1999; Fulton *et al*, 2006; Neil *et al*, 2008; Goepp *et al*, 2021). In our hand, with no TCR activators or co-stimulation, PGE_2 rather supports TGF-ß signaling (or vice-versa) as the simultaneous inhibition of both TGF-ß and PGE_2 signals synergistically prevented Treg induction.

An interesting finding in our study is the prominent induction of PGD_2 by both CLys and CSN from PBMC and monocytes. PGD_2 has both pro-inflammatory and resolving/anti-inflammatory effects, depending on the specific receptor engaged. It is considered anti-inflammatory when it complexes with the D-prostanoid receptor 1 (DP1 receptor) on myeloid cells but rather pro-inflammatory when it signals through DP2 receptor on CD4 T cells. Since we have shown a PGE_2-dependent conversion of CD4 T cells into Tregs, PGD_2 may potentially enhance inflammation by counter regulating this effect via T-cell-expressed DP2. However, it is very likely that, in our system, the pro-inflammatory effects of PGD_2 are masked by PGE_2 as has been shown elsewhere (Pettipher *et al*, 2007). Recently, another anti-inflammatory prostanoid, PGI_2, has been shown to drive Tregs in both human and mice via the repression of β-catenin signaling, thus preventing Treg reprogramming toward a pathogenic phenotype (Norlander *et al*, 2021). Mice deficient for the PGI_2 receptor IP had significantly enhanced OVA-elicited AAI in comparison to mice with intact PGI_2 signaling. Furthermore, macrophage-derived PGE_2 elicited by products of the helminth *H. polygyrus bakeri* has been implicated in the suppression of AAI. In this model, a switch from pro-inflammatory 5-lipoxygenase-derived eicosanoids to prostanoids triggered by parasite larval products mediated the suppression of AAI (de Los Reyes Jimenez *et al*, 2020). In line with these findings, we identified monocytes and macrophages as a major source of PGE_2 and IL-10, which synergized to drive Treg expansion. Recent advances have linked monocytes to both host defense and development of pathology during NCC (Uddin *et al*, 2010; Prabhakaran *et al*, 2017). We now show that monocytes licensed by viable parasite products are committed to promote a tolerogenic and suppressive environment as observed in peripheral blood of asymptomatic NCC patients, whereas products released during parasite death promoted an inflammatory phenotype with high expression of CD68 and CD80, markers associated with pathologies in multiple inflammatory diseases (Vatankhah *et al*, 2015; Pinto *et al*, 2019).

Very little is known about how cyst products regulate a tolerogenic phenotype in DC, macrophages, and monocytes and which active components are involved. Using mass spectrometry, we

identified the enzymes GDH and IDH in CLys and CSN as the main monocyte modulators that primed Treg induction from naïve CD4 T cells via PGE$_2$ and IL-10. Moreover, we noticed that, although significant, Treg induction by TsGDH is less potent compared to CLys and CSN. This might be potentially inherent to the protein expression system (e.g., post-translational architecture, incomplete protein folding) and/or absence of IDH activity, which was complementary to GDH-driven Treg induction in our system. Although the role of endogenous GDH and IDH has been extensively investigated in infectious diseases (e.g., malaria) before, its role in helminth infections remains elusive. Endogenous mammalian GDH is a hexameric enzyme that catalyzes the reversible conversion of glutamate to α-ketoglutarate, while IDH converts isocitrate to α-ketoglutarate. Additionally, IDH has implications for *de novo* genesis of cellular lipids and mediators (Metallo *et al*, 2011; Costello & Franklin, 2013). It is not clear at this stage how helminth GDH/IDH may stimulate monocyte receptors and how they may impact on the intracellular signaling events. We have recently identified *Hpb* GDH as a potent inducer of PGE$_2$ and IL-10, potentially via a MAP Kinase- and hypoxia-inducible factor-1α-dependent signaling (de Los Reyes Jimenez *et al*, 2020). Whether similar signaling events apply to monocytes in our system for PGE$_2$- and IL-10-driven Treg induction from CD4$^+$ T cells and whether and/or which cell surface receptors are involved warrants further investigation. As inhibitor experiments suggested that in our system IDH is rather complementary to GDH in inducing Tregs, it most likely provides an additional signal to the system, for example, via *de novo* production of PGE$_2$ or by further enhancing α-ketoglutarate levels. Another important facet of PGE$_2$ in this system is presumably the propagation of IL-10 production. Indeed, PGE$_2$ has been demonstrated to regulate the formation of IL-10 from monocytes, macrophages, or T cells (MacKenzie *et al*, 2013; Brencicova *et al*, 2017), thus, potentially, sustaining the induction of Tregs in local tissue milieu.

The presence of Tregs in the CNS of asymptomatic and severely affected NCC patients is currently viewed as a likely host mechanism, by which inflammatory responses are modulated in response to cystic lesions in the brain (Adalid-Peralta *et al*, 2012). As an important characteristic of CLys- and CSN-induced Tregs, we identified their capacity to proliferate and their putative CNS migratory signature by marked expression of CCR6 and CCR7. These homing receptors on CD4$^+$ T cells bind to CCL19, CCL20, and CCL21 on activated endothelial cells located at the BBB and drive the cells to extravasate into different compartments of the brain (e.g., parenchyma or subarachnoid space) via the choroid plexus (Wilson *et al*, 2010; Klein & Hunter, 2017). Thus, our data could shed light on the origin and migration of peripherally induced Tregs into the CNS. In the CNS, Tregs are rare during steady-state, but accumulate after various types of injury including stroke, brain lesions, and inflammatory insults (Liesz *et al*, 2009). Indeed, in our system, local induction of Tregs by viable cysts present in CNS may occur in NCC (Adalid-Peralta *et al*, 2012; Garcia *et al*, 2014b; Arce-Sillas *et al*, 2016) by a mechanism involving larval product-conditioned microglia. Tregs present in the CNS express high levels of FoxP3, but, distinct to peripherally induced Tregs, they express the serotonin receptor 5-HT7 and lectin-like receptor KLRG1 and are phenotypically active memory T cells (Xie *et al*, 2015; Ito *et al*, 2019). Besides limiting inflammation via IL-10 and CTLA-4 expression, Tregs in the CNS are induced by mechanisms involving STAT5 signaling and

local production of IL-2, IL-10, and IL-33 from astrocytes and microglia (Xie *et al*, 2015; Klein & Hunter, 2017; Ito *et al*, 2019) part of which was also found in our system. Deciphering further mechanistic aspects on the tissue level (brain) will require further studies.

Whereas IL-10 from CNS resident Tregs and microglia is considered to be anti-inflammatory and immunosuppressive (Burmeister & Marriott, 2018), the role of PGE$_2$ in the CNS is more complex. Conflicting reports using animal models deficient for PGE$_2$ receptors established multiple functions for PGE$_2$. The receptors EP1 and EP3 appear to have detrimental effects resulting in neuroinflammation, while EP2 and EP4 are rather neuroprotective and anti-inflammatory (Zhang & Rivest, 2001; McCullough *et al*, 2004; Saleem *et al*, 2009; Esaki *et al*, 2010). Importantly, PGE$_2$ has been shown to prevent Th1/Th17 polarization associated with increased levels of Tregs in experimental autoimmune encephalomyelitis (Liu *et al*, 2013), suggesting an important role for PGE$_2$ in the reciprocal pathway between Treg and Th17 cell induction. This Treg/Th17 functionality is further demonstrated by the significant upregulation of pro-inflammatory IL-1ß from PBMCs and microglia by both products derived from viable cysts as IL-1ß-mediated signals have been shown to preferentially drive the conversion of Tregs into Th17 (Deknuydt *et al*, 2009; Li *et al*, 2010). This feature could have important implications in certain patients harboring viable cysts in the brain but relatively lower levels of Tregs with little clinical manifestations (e.g., headaches) (Sotelo, 2011; Carpio *et al*, 2013). One study has revealed an association between increased PGE$_2$ levels in LPS-injured brain parenchyma and significantly reduced microglial activation, as well as IL-6 and TNFα expression (Zhang & Rivest, 2001). In line with these data, we noticed a differential activation of microglia in presence of both CLys and CSN as demonstrated by lower induction of Iba-1 expression alongside enhanced transcriptional levels of PGE$_2$, TNFα, IL-6, as well as IP-10 and CCL2, important attractants of CCR6$^+$ and CCR7$^+$ T cells (Stein & Nombela-Arrieta, 2005; Karpus, 2020), when compared to CVF, which solely induced TGF-β expression. This is indicative of the capacity of viable cysts and their actively secreted products to attract peripherally induced CCR6$^+$CCR7$^+$Tregs to the brain tissue or to induce *de novo* Treg locally from naïve CD4 T cells and thereby sustain an anti-inflammatory and thus asymptomatic state in some NCC patients.

Another finding is the unique property of CVF to promote the release of TGF-β from microglia. In rodent models and humans, the overexpression of this mediator and the association to its receptor (TGF-βR) resulted in phosphorylation of SMAD2/3 causing enhanced astrocyte and microglia activation and contributing to impairment of inhibitory synaptic transmission and induction of epileptic seizures and epilepsy (Bar-Klein *et al*, 2014; Weissberg *et al*, 2015). Thus, TGF-β induction in our model could suggest a similar process in the case of clinical NCC, wherein the severe inflammatory process in symptomatic patients is initiated when cysticerci die (either naturally or during anti-helminthic treatment), resulting in the release of the intravesicular fluid and a TGF-β-induced cascade leading to synaptogenesis and epileptogenesis. Furthermore, the loss of phagocytic activity of CVF-treated microglia suggests an additional mechanism leading to epileptic seizures, since maintenance of efficient microglial phagocytosis of apoptotic cells or degenerated neuronal debris is crucial to reduce CNS inflammation and to maintain healthy neuronal networks (Diaz-

Aparicio et al, 2020). Identifying the active TGF-ß inducer in CVF might be relevant in the treatment of NCC.

In conclusion, our findings identify a previously undescribed mechanism of Treg induction via the eicosanoid PGE_2 and IL-10 in helminth-induced immune regulation and provide new insights into understanding Treg function in asymptomatic NCC patients. Our findings also suggest a role for TGF-β from nonphagocytic microglia in the development of pathology (e.g., epileptic seizures/epilepsy) in symptomatic NCC patients and, thus, could potentially be a target for severe NCC. These findings open new perspectives into understanding immune regulation associated with symptomatic and asymptomatic NCC, which may eventually improve treatment strategies for patients suffering from NCC.

Materials and Methods

Animals and Taenia solium cyst products

C57BL/6 (WT) ($n = 8$) and OT-II mice (on a C57BL/6 background) ($n = 4$–5 per group), 6–8 weeks old, were respectively purchased from Envigo (Germany) or bred in-house and maintained under specific pathogen-free conditions in-house at the Institute of Medical Microbiology, Immunology, and Hygiene (MIH), TU Munich. All experiments were performed in accordance with and approved by local government authorities of Regierung von Oberbayern (Az. 55.1.54-2532-145-17).

Cysts of T. solium were harvested from the muscle tissue of a heavily infected pig at the School of Veterinary Medicine of the University of Zambia (ethical approval Ref. 2018-Mar-002/0005948). All collected cysts were initially washed extensively with sterile phosphate buffered saline (PBS) before further processing. For CVF preparation, cysts were placed into a sterile dish, cut open with a scalpel, and released fluid was collected, sterile filtered through 0.45 μm size filters, centrifuged (15,000 g for 60 min at 4°C), and aliquoted. To obtain whole cyst lysates (CLys), the cysts were homogenized and sonicated at 4°C and the supernatant obtained after centrifugation, as above, was sterile filtered and aliquoted. CSN was collected and pooled during 6 days of culture of 12–15 viable cysts/well in a six-well plate in 2 ml RPMI 1640 containing 10 mM HEPES buffer, 100 U/ml penicillin, 100 μg/ml streptomycin, 0.25 μg/ml amphotericin B, and 2 mM L-glutamine. 1 ml of supernatant was collected daily and replaced by fresh medium. All prepared materials were tested for endotoxin (levels < 0.05 EU/ml) and stored at −80°C until use.

Murine cell isolation, culture, and analysis

BMDCs, AM, splenocytes, and microglia were obtained from wild-type C57BL/6 mice and cultured as previously described in (Bhattacharjee et al, 2019), (Bang et al, 2011), (Layland et al, 2010) and (Kolter et al, 2019), respectively.

BMDCs were obtained as previously described (Bhattacharjee et al, 2019). Briefly, femurs and tibiae were isolated from mice's muscle tissue under sterile conditions. Bones were opened at both ends and the bone marrow was flushed out and washed with sterile PBS. Cell preparations were depleted of erythrocyte with Tris-Buffered Ammonium Chloride buffer (ACT), filtered over a 100 μm strainer, washed, and seeded into bacteriological petri dishes at 5×10^5/ml in 10 ml complete medium (RPMI 1640 (Sigma-Aldrich) supplemented with 10% heat-inactivated and filtered FCS (Sigma-Aldrich), 1% penicillin/streptomycin (Life Technologies), 50 mM 2-ME (Sigma-Aldrich), and 20 ng/ml GM-CSF (Miltenyi Biotec)) and incubated at 37°C in a 5% CO_2 atmosphere. 10 ml of complete medium was added to each petri dish on day 3, and on day 6, half of the culture supernatant was collected, centrifuged at 300 g, 8 min, 4°C and the cell pellet was resuspended in fresh complete medium and added to the dish. At day 7, BMDCs ($\geq$ 86% CD11c$^+$ cells) were harvested, plated at 1×10^6/ml cells, and pre-exposed to 10 μg/ml CVF, CLys, and CSN for 72 h before stimulation with 50 ng/ml ultrapure LPS (Escherichia coli 055:B5 strain; Sigma-Aldrich). Alternatively, BMDCs were incubated simultaneously with the cyst products and LPS. After 24 h of stimulation, supernatants were collected and analyzed for cytokine secretion by ELISA (TNFα, IL-6, IL-10, eBioscience or R&D Systems) and expression of costimulatory and surface markers was determined by flow cytometry (FACS) on a CytoFLEX S (Beckman Coulter) using the following antibodies following FcR-Block: CD11c (clone N418), CD80 (clone 16-10A1), CD86 (clone GL-1) (all from BioLegend), and MHCII (clone M5/114.15.2) (eBioscience). Live cells, analyzed with Zombie NIR viability kit (BioLegend), were routinely $\geq$ 83%.

AM were isolated as reported previously (Bang et al, 2011). Briefly, bronchoalveolar lavage (BAL) was performed and the recovered fluid was centrifuged; pelleted cells were then resuspended in RPMI-1640 medium supplemented with 10% FCS and 1% penicillin/streptomycin and incubated for 2 h at 37°C, 5% CO_2. Nonadherent cells were removed and AM ($\geq$ 80% CD11b$^+$, F4/80$^+$ cells) were stimulated as indicated for BMDCs. Cytokines (TNFα, TGF-ß, IL-10) in supernatant were evaluated and the relative cell morphology and shape was analyzed using ImageJ, version 2.0.0 (NIH, MD). Subsequently, AM and BMDCs were analyzed via FACS for early (Annexin V$^+$/PI$^-$) and late (Annexin V$^-$/PI$^+$) apoptotic (necrotic) and dead (Annexin V$^+$/PI$^+$) cells using Annexin V/PI staining kit (BioLegend).

Spleen cells were obtained as previously described (Layland et al, 2010) by grinding through a 70 μm-mesh cell strainer and incubated with CVF, CLys, and CSN for 72 h. The induction of regulatory T cells (CD4$^+$CD25^{hi}FoxP3$^+$ cells) was analyzed by FACS using CD3 (clone 17A2), CD8a (clone 53-6.7), CD25 (clone PC61.5), FoxP3 (clone FJK-16S), (all from eBioscience), and CD4 (clone GK1.5) (BioLegend) after fixing/permeabilizing cells with eBioscience FoxP3 transcription factor staining buffer set (Thermofisher Scientific).

Microglia were generated from newborn mice (P1-3) as described previously (Kolter et al, 2019). The mice were decapitated, the olfactory bulbs, cerebellum were removed, as well as meninges and choroid plexus. Tissue was dissociated and filtered through 100 ul cell strainer. Cells were centrifuged for 5 min at 450 g at 4°C. The cell pellet was resuspended in 5 ml of DMEM high glucose (10% FCS, 0.5% Ciprofloxacin) (Gibco) and plated on a T25 culture flask, which was previously coated overnight with 5 μg/ml Poly-L-Lysine. The T25 culture flasks were incubated for around 10 days with repeated medium exchange at 37°C in a 5% CO_2 humidified incubator. 48 h before further analysis, 20 ng/ml of M-CSF (Pepro-Tech) was added to the cultures. The cultures were trypsinized in 0.05% Trypsin-EDTA for 15 min at 37°C, washed

with medium, scraped, and seeded to appropriate plate for downstream analysis. For cell stimulation, 0.5–1 × 10^6/ml were seeded in cell culture plates (Thermo Fisher Scientific). After resting overnight, cells were stimulated with 10 µg/ml CVF, CLys, or CSN for 24 h (flow cytometry, RT–PCR, immunofluorescence microscopy) or 24–72 h (PGE$_2$ Enzyme immunoassay (Cayman Chemical)).

For flow cytometry, cells were washed with staining buffer (2 mM EDTA and 2% FCS in PBS), and stained for 30 min at 4°C in 100 µl volume. FcγRII/III were blocked by prior incubation with anti-CD16/32 antibody (eBioscience). Subsequently, cells were washed and analyzed with a 10-color flow cytometer (Gallios; Beckman Coulter) and the Kaluza software (version 1.5a; Beckman Coulter). Anti-mouse antibodies CD11b-PE-Cy7; MHCII-eFluor 450; CD45-PE (all from eBioscience) were used.

For Treg induction experiments, CVF-, CLys-, and CSN-microglia culture supernatants were used, in the presence of anti-CD3/CD28 antibody (1 µg/ml; BioLegend), to stimulate naïve CD4$^+$CD62L$^{+/hi}$, purified from mice lymph nodes using CD4$^+$CD62L$^+$ T cell isolation kit II (Miltenyi Biotec), for 72 h and Treg induction assessed as above mentioned.

For microscopy, cells were seeded in an eight-well poly-L-lysine–treated m-slide (ibidi) and incubated with CVF, CLys, and CSN at 37°C for 24 h. Cells were then fixed in 4% PFA, washed twice with PBS, and subsequently permeabilized with 0.1% Triton-X in PBS. Blocking and staining was done with 1% BSA and 0.1% Tween 20 in PBS. Cells were then stained with Iba-1-635 (Wako), phalloidin-AF488 (Invitrogen), and DAPI for 15 min, washed, and mounted with mounting medium (Dako) for microscopic analysis with the LSM880. Pictures were analyzed and edited using the ZEN black and Imaris software.

For RT–PCR, RNA was extracted from microglia using the Extractme Total RNA Micro Spin kit according to manufacturer's instruction (Blirt). RNA was reversely transcribed to cDNA with the SuperScriptTM IV VILO mix (Thermo Fisher). qRT–PCR was performed with ABsolute qPCR SYBR Green (Thermo Fisher Scientific) at the LightCycler 480 (Roche). The primers used are shown in Table 1.

For the phagocytosis assay, red-fluorescent 1 µm latex beads (Sigma-Aldrich) were pre-opsonized in FBS for 1 h at 37°C and afterward diluted with DMEM to reach the final concentrations for beads and FBS in DMEM of 0.01% (v/v) and 0.05% (v/v), respectively (approximately 25,000 beads/ml). 200 µl of bead-containing

DMEM was either added to microglial culture seeded in a 24-well flat bottom plate (Thermo Fisher Scientific) or poly-L-lysine-treated m-slide (ibidi), respectively. Cultures were incubated at 37°C for 1 h, then thoroughly washed five times with ice-cold PBS and fixed with 4% PFA for further staining for microscopy.

Adoptive transfer and *in vivo* Treg priming

BMDCs were generated as above and incubated for 72 h with CVF or CLys. 24 h before the end of culture, cells were pulsed overnight with endotoxin-free OVA protein (20 µg/ml). On day 0, CVF- and CLys-treated BMDCs were extensively washed with PBS, and 2 × 10^5 antigen-pulsed cells, or PBS or naive BMDCs as control, were subcutaneously injected into separate recipient C57BL/6 mice, which had previously (24 h earlier) received intraperitoneally 1–2 × 10^5 flow sorted naïve CD4$^+$CD44$^{-/lo}$ OT-II cells. Mice were sacrificed on day 7, the inguinal lymph nodes (ILN) were removed and ILN cell suspensions, prepared as previously reported (Layland et al, 2010), were stained with CD4 (clone GK 1.5) (BioLegend), CD45.1 (clone A20), CD25 (clone PC61), FoxP3 (clone MF23) (all from BD Biosciences), and Granzyme B (clone NGZB) (eBioscience) for flow cytometry analysis of Treg induction.

Human cell isolation, culture, and analysis

The study was approved by the local ethical committee of the Technical University of Munich (Reference: 215/18S) and all individuals included ($n = 8$) in the study consented for enrollment.

PBMCs, monocytes, and monocyte-derived macrophages (MDM) were obtained from peripheral blood of healthy volunteers from mixed genders by density gradient centrifugation and as previously reported (de Los Reyes Jimenez et al, 2020). Monocyte isolation from whole blood was performed using a RosetteSep Human Monocyte Enrichment Cocktail kit (StemCell Technologies) and naïve CD4 T cells enriched with the naïve CD4$^+$ T cell isolation kit II (Miltenyi Biotec) strictly according to the manufacturer's protocol. The purity of monocytes, evaluated by FACS staining with CD14 (clone HCD14) (BioLegend), was routinely ≥ 85%. The monocyte negative fractions were depleted of erythrocytes via ACT buffer lysis. MDM were generated from enriched monocytes in the presence of 50 ng/ml of rhGM-CSF for 7 days with exchange of 50% of medium at day 3 and 5 by fresh medium.

Table 1. Sequence and genotyping primers for microglial functional studies.

Gene	Forward Primer (5′-3′)	Reverse Primer (5′-3′)
Gapdh	ACTCCACTCACGGCAAATTC	TCTCCATGGTGGTGAAGACA
Tnfα	TCGTAGCAAACCACCAAGTG	CCTTGTCCCTTGAAGAGAACC
Il-1ß	TTCAGGCAGGCAGTATCACTC	GAAGGTCCACGGGAAAGACAC
Il-6	GACAAAGCCAGAGTCCTTCAGAGAG	CTAGGTTTGCCGAGTAGATCTC
Ip-10	GGATCCCTCTCGCAAGGA	ATCGTGGCAATGATCTCAACA
Ccl2	AGCCAACTCTCACTGAAGCC	GCTTGGTGACAAAAACTACAGC
Tgf-ß	GCAACATGTGGAACTCTACCAGAA	GACGTCAAAAGACAGCCACTC
Il-10	CCCTTTGCTATGGTGTCCTT	TGGTTTCTCTTCCCAAGACC

Monocyte negative (Mo^{neg}) (2.5×10^5 cells) (or naïve CD4 T cells) and positive (Mo^{pos}) fractions (2×10^5 cells) (1:4 Mo/CD4 T cells ratio) from the same donor as well as PBMCs and MDM were cultured with 10 µg/ml CVF, CLys, and CSN or 5 µg/ml *Taenia solium* GDH (TsGDH) or rhGDH (10 µg/ml (abx066819) (Abbexa)) for 24 or 72 h. CLys- and CSN-monocyte culture supernatants were used, in the presence of anti-CD3/CD28 antibody (1 µg/ml (BioLegend), to stimulate naïve CD4$^+$ T cells. Culture supernatants were collected for cytokine and bioactive lipid mediator analysis (detailed below). Cytokine concentrations were determined using a 10-plex panel (IL-1b, TNFα, IFNγ, IL-4, IL-6, IL-10, IL-13, IL-17A, IP-10, CCL2) human magnetic LUMINEX assay (R&D Systems) according to the instructions in the pre-optimized protocol provided by the manufacturer and collected data were analyzed on a Bio-Plex 200 instrument equipped with Bio-Plex Manager software version 6.2 (Bio-Rad). The induction and characterization of Tregs (CD4$^+$CD127$^-$CD25^{hi}FoxP3$^+$CTLA4$^+$ cells) was assessed with the following antibodies: CD3 (clone UCHT1), CD4 (clone RPA-T4), CD127 (clone A019D5), CD25 (clone BC96), CTLA-4 (clone L3D10), IFNγ (clone 4S.B3) (all from BioLegend), and FoxP3 (clone PCH101) (Invitrogen) and the phenotypic functional markers of stimulated monocytes (CD14 (clone HCD14), CD68 (clone Y1/82A), CD80 (clone (2D10), CD163 (clone GHI/61), CD226 (clone 11A8)) evaluated by FACS. For cytokine staining, cells were cultured in the presence of GolgiStop (BD Biosciences) or Brefeldin A (Sigma-Aldrich) for the last 4 h of culture and fixed with Cytofix/Cytoperm buffer (BD Biosciences) after surface staining. The expression of trafficking receptors on Treg was evaluated with CXCR3 (clone G025H7), CCR4 (clone L291H4), CCR6 (clone G034E3) (all from BioLegend), and CCR7 (clone 150503) (BD Biosciences). For blocking experiments, PBMCs or Mo^{pos} - Mo^{neg} cocultures were preincubated with mPGES1 inhibitor (934, 10 µM, provided by Prof. Per-Johan Jakobsson) or PGE$_2$ receptor EP2 (PF-04418948, 1 µM) and EP4 (CJ-42794, 1 µM) (Cayman Chemical) antagonists and/or inhibitors of IL-10 (clone 3F9, 10 µg/ml) (BioLegend) and TGF-ß (SB431542, 5 µM) (Tocris Bioscience) receptors or DMSO as a control before stimulation with CVF, CLys, or CSN and analysis of Treg induction after 72 h. For GDH and IDH signaling inhibition, cells were preincubated with Bithionol (20 µM (Sigma-Aldrich)) and/or IDH305 (50 nM (Cayman Chemical). When indicated, CLys or CSN was pretreated overnight at 37°C with proteinase K (PK, 100 µg/ml) (Sigma-Aldrich) before stimulation with PBMC. For Treg induction by PGE$_2$ and IL-10, PBMCs were incubated for 72 h with PGE$_2$ analog dinoprostone (14010, 5 µM (Cayman Chemical)) and/or recombinant human IL-10 (rhIL-10) (130-093-948, 10 ng/ml; Miltenyi Biotec).

Real-time PCR

Monocyte-derived macrophages (MDM) were lysed in RLT Buffer (Qiagen), with 1% β-mercaptoethanol (Merck Millipore) followed by RNA extraction (Zymo Research) and reverse transcription according to the manufacturer's instructions (Thermo Fisher Scientific). qPCR analysis was performed as described previously (Dietz *et al*, 2017) using the primers in Table 2.

LC-MS/MS lipid mediator analysis

Supernatant collected from cell culture was stored with 50% MeOH at −80°C. Lipid mediator analysis was performed as described previously by Henkel *et al* (2019). Automated solid phase extractions were performed with a Microlab STAR robot (Hamilton). Prior to extraction, all samples were diluted with H$_2$O to a MeOH content of 15% and 10 µl of IS stock solution was added. Samples were extracted using Strata-X 96-well plates (30 mg, Phenomenex) and eluted with MeOH. Samples were evaporated to dryness under N$_2$ stream and redissolved in 100 µl MeOH/H$_2$O (1:1).

Chromatographic separation of eicosanoids was achieved with a 1260 Series HPLC (Agilent) using a Kinetex C18 reversed phase column (2.6 µm, 100×2.1 mm, Phenomenex) with a SecurityGuard Ultra Cartridge C18 (Phenomenex) precolumn. The QTRAP 5500 mass spectrometer (Sciex), equipped with a Turbo-V^{TM} ion source, was operated in negative ionization mode. Samples were injected via an HTC PAL autosampler (CTC Analytics), set to 7.5°C. Identification of metabolites was achieved via retention time and scheduled multiple reaction monitoring (sMRM) as previously specified. Acquisition of LC-MS/MS data was performed using Analyst Software 1.6.3 followed by quantification with MultiQuant Software 3.0.2 (both from Sciex).

Mass spectrometry analysis

For mass spectrometry analysis, 100 µl of the cyst material (CVF, CLys, CSN) was reduced by addition of 10 µl of 50 mM of DTT solution and incubation for 30 min at 60°C. Alkylation was carried out by addition of 10 µl of 150 mM freshly prepared iodacetamide an incubation for 30 min at room temperature in the dark. For tryptic digest, 10 µl of trypsin solution (50 µg/ml) was added and the sample was incubated for 16 h at 37°C. After addition of 100 µl of 0.1% formic acid solution and 200 µl of acetonitrile, the samples were evaporated to dryness in a speed vac (DNA 120, Thermo Scientific) and stored at −80°C. For MS analysis, the samples were dissolved by adding 30 µl of 0.1% formic acid and sonication for 15 min. The samples were then filtered through a 0.22-µm centrifuge filter (Millipore). Peptides were loaded onto an Acclaim PepMap RSLC C18 trap column (Trap Column, NanoViper, 75 µm × 20 mm, C18, 3 µm, 100 Å, Thermo-Fisher Scientific) with a flow rate of 5 µl/min and separated on a PepMap RSLC C18 column (75 µm × 500 mm, C18, 2 µm, 100 Å, ThermoFisher Scientific) at a flow rate of 0.3 µl/min. A linear gradient from 5% (vol/vol) to 35% (vol/vol) buffer B (acetonitrile with 0.1% formic acid) in 67 min eluted the peptides to an Orbitrap

Table 2. Sequence and genotyping primers for lipid mediator enzymes in MDM.

Gene	Forward Primer (5′-3′)	Reverse Primer (5′-3′)
PTGS2	GCTGGAACATGGAATTACCCA	CTTTCTGTACTGCGGGTGGAA
PTGES	TCAAGATGTACGTGGTGGCC	GAAAGGAGTAGACGAAGCCCAG
ALOX5	GATTGTCCCCATTGCCATCC	AGAAGGTGGGTGATGGTCTG
ALOX15	GGACACTTGATGGCTGAGGT	GTATCGCAGGTGGGGAATTA
GAPDH	GAAGGTGAAGGTCGGAGT	GAAGATGGTGATGGGATTTC
MRC1	CGATCCGACCCTTCCTTGAC	TGTCTCCGCTTCATGCCATT

QExactive plus mass spectrometer (ThermoFisher Scientific). Full scans and five dependent collision-induced dissociation MS2 scans were recorded in each cycle. The mass spectrometry data derived from the SEC fractions were searched using WormBase Parasite database for *T. solium* (Version WS276, October 2020) and against the Swiss-Prot *Taenia solium* database downloaded from UniProt (18. March 2019 edition) using the Sequest HT Algorithm implemented into the "Proteome Discoverer 1.4" software (ThermoFisher Scientific). The search was limited to tryptic peptides containing a maximum of two missed cleavage sites and a peptide tolerance of 10 ppm for precursors and 0.04 Da for fragment masses. Proteins were identified with one distinct peptide with a target false discovery rate for peptides below 1% according to the decoy search. For further evaluation, three independent datasets resulting from biological replicates were compared. Functions of identified proteins were screened for PGE$_2$ and IL-10 using Gene Ontology (February 1, 2020 release).

Expression and purification of TsGDH and activity

The full length gene, encoding the fused exons of *T. solium* GDH (TsM_000572800; https://parasite.wormbase.org) was synthesized by GeneArt (Regensburg, Germany). For expression in *E. coli*, the gene was optimized in codon usage and inserted between the NdeI and XhoI site of the pET28b vector (Invitrogen molecular probes, Darmstadt, Germany), generating an N-terminal His6-Tag followed by a thrombin cleavage site. The protein was expressed in *E. coli* JM109 (DE3) (Promega, Wisconsin, USA) cells, grown in LB medium (Serva, Heidelberg, Germany) supplemented with 35 mg kanamycin and 2.5% (v/v) ethanol at 37°C to an OD600 of ~ 0.6 prior to the induction with 1 mM IPTG. After induction, the cells were further cultivated at 20°C for 16 h. Cells were harvested by centrifugation at 10,000 *g* (Beckman Avanti J-26 XP, Beckman Coulter, Brea, USA) for 20 min at 4°C, washed one time, and then resuspended with buffer A (50 mM Tris/HCl, 300 mM NaCl, 20 mM imidazole, 2.5% (v/v) glycerol, 0.1 mM TCEP, pH 8.0) supplemented with DNase I (AppliChem, Darmstadt, Germany) and Protease Inhibitor Mix HP (Serva, Heidelberg, Germany) prior to lysis in a Basic Z cell disrupter operated at 2.3 kbar (Constant Systems, Warwick, UK). After separation of insoluble material by centrifugation for 30 min at 45,000 *g* at 4°C, the cleared lysate was applied onto a 5 ml HisTrap FF-column (GE Healthcare, Munich, Germany), pre-equilibrated with buffer A, operated on an Äkta Explorer (GE Healthcare, Munich, Germany) at 4°C applying a flow rate of 3 ml/min. After loading of the lysate, the column was washed with buffer A until a stable baseline was reached (monitored at 280 nm). Bound proteins were eluted stepwise in 15%, 25%, and 100% of buffer B (50 mM Tris–HCl, 300 mM NaCl, 500 mM imidazole, 2.5% (v/v) glycerol, 0.1 mM TCEP, pH 8.0). Fractions containing TsGDH were pooled and dialyzed over night to buffer C (20 mM Hepes/KOH, 20 mM NaCl, 2.5% (v/v) glycerol, pH 6.8). The protein was further purified by anion-exchange chromatography using a 6 ml resource Q column (GE Healthcare, Munich, Germany) pre-equilibrated in buffer C. After protein loading, the column was washed with 5 column volumes (CV) of buffer C and eluted with a linear gradient of 15 CV to buffer D (20 mM Hepes/KOH, 1 M NaCl, 2.5% (v/v) glycerol, pH 6.8). In case a further purification step applying cation-exchange chromatography using a 1 ml Resource S column (GE Healthcare, Munich, Germany) was performed, following the same protocol as for the anion-exchange chromatography. The purity of

TsGDH containing fractions was analyzed by SDS–PAGE. The protein was pooled and dialyzed against PBS, flash frozen in liquid nitrogen, and stored at −20°C until used. The enzymatic activity of TsGDH was assessed using the GDH activity assay kit (MAK099, Merck) following manufacturer's recommendations and bioactivity tested using different concentrations (1, 5, 10, 20 μg/ml). LPS levels were quantified and not detectable (levels < 0.005 EU/ml).

ELISA, enzyme immunoassays (EIA) and LUMINEX assay

PGE$_2$ concentrations in PBMC, monocyte, macrophage, and microglia culture supernatants were determined with commercially available enzyme immunoassay kits (Cayman Chemical), according to the manufacturer's instruction. For IL-10 levels, the human ELISA Set (BD Biosciences) was used according to the manufacturer's instructions. Cytokine concentrations with human samples were determined using a 10-plex panel (IL-1b, TNFα, IFNγ, IL-4, IL-6, IL-10, IL-13, IL-17A, IP-10, CCL2) human magnetic LUMINEX assay (R&D Systems) according to the instructions in the pre-optimized protocol provided by the manufacturer and collected data were analyzed on a Bio-Plex 200 instrument equipped with Bio-Plex Manager software version 6.2 (Bio-Rad).

Statistical analysis

The data were converted to heat maps using Excel, Version 16.16. 27 (Microsoft). Statistical analysis was performed using the software Prism 9, Version 9.0.1 (GraphPad Software, Inc., La Jolla, USA). Comparative analysis among groups was conducted using a Kruskal–Wallis test with a Dunn's nonparametric *post hoc* test (> 2 groups). In case of two groups, a Mann–Whitney U test was used. Statistical significance was accepted when $P < 0.05$.

Data availability

This study includes no data deposited in external repositories.

Expanded View for this article is available online.

Author contributions

Ulrich Fabien Prodjinotho: Conceptualization; Data curation; Formal analysis; Validation; Investigation; Visualization; Methodology; Writing – original draft; Writing – review & editing. **Vitka Gres:** Data curation; Formal analysis; Validation; Investigation; Visualization; Methodology; Writing – review & editing. **Fiona, DR Henkel:** Data curation; Formal analysis; Validation; Investigation; Visualization; Methodology; Writing – review & editing. **Matthew Lacorcia:**

References

Adalid-Peralta L, Arce-Sillas A, Fragoso G, Cardenas G, Rosetti M, Casanova-Hernandez D, Rangel-Escareno C, Uribe-Figueroa L, Fleury A, Sciutto E (2013) Cysticerci drive dendritic cells to promote *in vitro* and *in vivo* Tregs differentiation. *Clin Dev Immunol* 2013: 981468

Adalid-Peralta L, Fleury A, Garcia-Ibarra TM, Hernandez M, Parkhouse M, Crispin JC, Voltaire-Proano J, Cardenas G, Fragoso G, Sciutto E (2012) Human neurocysticercosis: *in vivo* expansion of peripheral regulatory T cells and their recruitment in the central nervous system. *J Parasitol* 98: 142–148

Aloisi F (2001) Immune function of microglia. *Glia* 36: 165–179

Arce-Sillas A, Álvarez-Luquín DD, Cárdenas G, Casanova-Hernández D, Fragoso G, Hernández M, Proaño Narváez JV, García-Vázquez F, Fleury A, Sciutto E *et al* (2016) Interleukin 10 and dendritic cells are the main suppression mediators of regulatory T cells in human neurocysticercosis. *Clin Exp Immunol* 183: 271–279

Badur MG, Muthusamy T, Parker SJ, Ma S, McBrayer SK, Cordes T, Magana JH, Guan KL, Metallo CM (2018) Oncogenic R132 IDH1 mutations Limit NADPH for *de novo* lipogenesis through (D)2-hydroxyglutarate production in fibrosarcoma cells. *Cell Rep* 25: 1680

Bang BR, Chun E, Shim EJ, Lee HS, Lee SY, Cho SH, Min KU, Kim YY, Park HW (2011) Alveolar macrophages modulate allergic inflammation in a murine model of asthma. *Exp Mol Med* 43: 275–280

Bar-Klein G, Cacheaux LP, Kamintsky L, Prager O, Weissberg I, Schoknecht K, Cheng P, Kim SY, Wood L, Heinemann U *et al* (2014) Losartan prevents acquired epilepsy via TGF-beta signaling suppression. *Ann Neurol* 75: 864–875

Barrett NA, Rahman OM, Fernandez JM, Parsons MW, Xing W, Austen KF, Kanaoka Y (2011) Dectin-2 mediates Th2 immunity through the generation of cysteinyl leukotrienes. *J Exp Med* 208: 593–604

Betz M, Fox BS (1991) Prostaglandin E2 inhibits production of Th1 lymphokines but not of Th2 lymphokines. *J Immunol* 146: 108–113

Bhattacharjee S, Mejias-Luque R, Loffredo-Verde E, Toska A, Flossdorf M, Gerhard M, Prazeres da Costa C (2019) Concomitant Infection of *S. mansoni* and *H. pylori* promotes promiscuity of antigen-experienced cells and primes the liver for a lower fibrotic response. *Cell Rep* 28: 231–244 e235

Boniface K, Bak-Jensen KS, Li Y, Blumenschein WM, McGeachy MJ, McClanahan TK, McKenzie BS, Kastelein RA, Cua DJ, de Waal MR (2009) Prostaglandin E2 regulates Th17 cell differentiation and function through cyclic AMP and EP2/EP4 receptor signaling. *J Exp Med* 206: 535–548

Brencicova E, Jagger AL, Evans HG, Georgouli M, Laios A, Attard Montalto S, Mehra G, Spencer JO, Ahmed AA, Raju-Kankipati S *et al* (2017) Interleukin-10 and prostaglandin E2 have complementary but distinct suppressive effects on Toll-like receptor-mediated dendritic cell activation in ovarian carcinoma. *PLoS One* 12: e0175712

Burmeister AR, Marriott I (2018) The interleukin-10 family of cytokines and their role in the CNS. *Front Cell Neurosci* 12: 458

Cardenas G, Fragoso G, Rosetti M, Uribe-Figueroa L, Rangel-Escareno C, Saenz B, Hernandez M, Sciutto E, Fleury A (2014) Neurocysticercosis: the effectiveness of the cysticidal treatment could be influenced by the host immunity. *Med Microbiol Immunol* 203: 373–381

Carmen-Orozco RP, Dávila-Villacorta DG, Cauna Y, Bernal-Teran EG, Bitterfeld L, Sutherland GL, Chile N, Céliz RH, Ferrufino-Schmidt MC, Gavídia CM *et al* (2019) Blood-brain barrier disruption and angiogenesis in a rat model for neurocysticercosis. *J Neurosci Res* 97: 137–148

Carpio A, Fleury A, Hauser WA (2013) Neurocysticercosis: five new things. *Neurol Clin Pract* 3: 118–125

Cho KS, Lee JH, Park MK, Park HK, Yu HS, Roh HJ (2015) Prostaglandin E2 and transforming growth factor-beta play a critical role in suppression of allergic airway inflammation by adipose-derived stem cells. *PLoS One* 10: e0131813

Costello LC, Franklin RB (2013) A review of the important central role of altered citrate metabolism during the process of stem cell differentiation. *J Regen Med Tissue Eng* 2: 1

Crittenden S, Goepp M, Pollock J, Robb CT, Smyth DJ, Zhou Y, Andrews R, Tyrrell V, Gkikas K, Adima A *et al* (2021) Prostaglandin E2 promotes intestinal inflammation via inhibiting microbiota-dependent regulatory T cells. *Sci Adv* 7: eabd7954

Deknuydt F, Bioley G, Valmori D, Ayyoub M (2009) IL-1beta and IL-2 convert human Treg into T(H)17 cells. *Clin Immunol* 131: 298–307

Dennis EA, Norris PC (2015) Eicosanoid storm in infection and inflammation. *Nat Rev Immunol* 15: 511–523

Devinsky O, Vezzani A, O'Brien TJ, Jette N, Scheffer IE, de Curtis M, Perucca P (2018) Epilepsy. *Nat Rev Dis Primers* 4: 18024

Diaz-Aparicio I, Paris I, Sierra-Torre V, Plaza-Zabala A, Rodríguez-Iglesias N, Márquez-Ropero M, Beccari S, Huguet P, Abiega O, Alberdi E *et al* (2020) Microglia actively remodel adult hippocampal neurogenesis through the phagocytosis secretome. *J Neurosci* 40: 1453–1482

Dietz K, de Los Reyes Jiménez M, Gollwitzer ES, Chaker AM, Zissler UM, Rådmark OP, Baarsma HA, Königshoff M, Schmidt-Weber CB, Marsland BJ *et al* (2017) Age dictates a steroid-resistant cascade of Wnt5a, transglutaminase 2, and leukotrienes in inflamed airways. *J Allergy Clin Immunol* 139: 1343–1354.e6

English K, Ryan JM, Tobin L, Murphy MJ, Barry FP, Mahon BP (2009) Cell contact, prostaglandin E(2) and transforming growth factor beta 1 play non-redundant roles in human mesenchymal stem cell induction of CD4+CD25(High) forkhead box P3+ regulatory T cells. *Clin Exp Immunol* 156: 149–160

Esaki Y, Li Y, Sakata D, Yao C, Segi-Nishida E, Matsuoka T, Fukuda K, Narumiya S (2010) Dual roles of PGE2-EP4 signaling in mouse experimental autoimmune encephalomyelitis. *Proc Natl Acad Sci U S A* 107: 12233–12238

Esser-von Bieren J (2019) Eicosanoids in tissue repair. *Immunol Cell Biol* 97: 279–288

Fleury A, Cardenas G, Adalid-Peralta L, Fragoso G, Sciutto E (2016) Immunopathology in *Taenia solium* neurocysticercosis. *Parasite Immunol* 38: 147–157

Fujita M, Mahanty S, Zoghbi SS, Ferraris Araneta MD, Hong J, Pike VW, Innis RB, Nash TE (2013) PET reveals inflammation around calcified *Taenia solium* granulomas with perilesional edema. *PLoS One* 8: e74052

Fulton AM, Ma X, Kundu N (2006) Targeting prostaglandin E EP receptors to inhibit metastasis. *Cancer Res* 66: 9794–9797

Garcia HH, Nash TE, Del Brutto OH (2014a) Clinical symptoms, diagnosis, and treatment of neurocysticercosis. *Lancet Neurol* 13: 1202–1215

Garcia HH, Rodriguez S, Friedland JS, Cysticercosis Working Group in Peru (2014b) Immunology of *Taenia solium* taeniasis and human cysticercosis. *Parasite Immunol* 36: 388–396

Goepp M, Crittenden S, Zhou Y, Rossi AG, Narumiya S, Yao C (2021) Prostaglandin E2 directly inhibits the conversion of inducible regulatory T cells through EP2 and EP4 receptors via antagonizing TGF-beta signalling. *Immunology* 164: 777–791

Grainger JR, Smith KA, Hewitson JP, McSorley HJ, Harcus Y, Filbey KJ, Finney CA, Greenwood EJ, Knox DP, Wilson MS *et al* (2010) Helminth secretions induce *de novo* T cell Foxp3 expression and regulatory function through the TGF-beta pathway. *J Exp Med* 207: 2331–2341

Harris SG, Padilla J, Koumas L, Ray D, Phipps RP (2002) Prostaglandins as modulators of immunity. *Trends Immunol* 23: 144–150

Henkel FDR, Friedl A, Haid M, Thomas D, Bouchery T, Haimerl P, de Los Reyes Jiménez M, Alessandrini F, Schmidt-Weber CB, Harris NL *et al* (2019) House dust mite drives proinflammatory eicosanoid reprogramming and macrophage effector functions. *Allergy* 74: 1090–1101

Ito M, Komai K, Mise-Omata S, Iizuka-Koga M, Noguchi Y, Kondo T, Sakai R, Matsuo K, Nakayama T, Yoshie O *et al* (2019) Brain regulatory T cells suppress astrogliosis and potentiate neurological recovery. *Nature* 565: 246–250

James MJ, Penglis PS, Caughey GE, Demasi M, Cleland LG (2001) Eicosanoid production by human monocytes: does COX-2 contribute to a self-limiting inflammatory response? *Inflamm Res* 50: 249–253

Kaisar MMM, Ritter M, del Fresno C, Jónasdóttir HS, van der Ham AJ, Pelgrom LR, Schramm G, Layland LE, Sancho D, Prazeres da Costa C *et al* (2018) Dectin-1/2-induced autocrine PGE2 signaling licenses dendritic cells to prime Th2 responses. *PLoS Biol* 16: e2005504

Karpus WJ (2020) Cytokines and chemokines in the pathogenesis of experimental autoimmune encephalomyelitis. *J Immunol* 204: 316–326

Klein RS, Hunter CA (2017) Protective and pathological immunity during central nervous system infections. *Immunity* 46: 891–909

Kolter J, Feuerstein R, Zeis P, Hagemeyer N, Paterson N, d'Errico P, Baasch S, Amann L, Masuda T, Lösslein A *et al* (2019) A subset of skin macrophages contributes to the surveillance and regeneration of local nerves. *Immunity* 50: 1482–1497.e7

Lan Q, Fan H, Quesniaux V, Ryffel B, Liu Z, Zheng SG (2012) Induced Foxp3(+) regulatory T cells: a potential new weapon to treat autoimmune and inflammatory diseases? *J Mol Cell Biol* 4: 22–28

Lan X, Han X, Li Q, Yang QW, Wang J (2017) Modulators of microglial activation and polarization after intracerebral haemorrhage. *Nat Rev Neurol* 13: 420–433

Layland LE, Mages J, Loddenkemper C, Hoerauf A, Wagner H, Lang R, da Costa CU (2010) Pronounced phenotype in activated regulatory T cells during a chronic helminth infection. *J Immunol* 184: 713–724

Layland LE, Straubinger K, Ritter M, Loffredo-Verde E, Garn H, Sparwasser T, Prazeres da Costa C (2013) Schistosoma mansoni-mediated suppression of allergic airway inflammation requires patency and Foxp3+ Treg cells. *PLoS Negl Trop Dis* 7: e2379

Li L, Kim J, Boussiotis VA (2010) IL-1beta-mediated signals preferentially drive conversion of regulatory T cells but not conventional T cells into IL-17-producing cells. *J Immunol* 185: 4148–4153

Li Y, Severance EG, Viscidi RP, Yolken RH, Xiao J (2019) Persistent toxoplasma infection of the brain induced neurodegeneration associated with activation of complement and microglia. *Infect Immun* 87: e00139-19

Liesz A, Suri-Payer E, Veltkamp C, Doerr H, Sommer C, Rivest S, Giese T, Veltkamp R (2009) Regulatory T cells are key cerebroprotective immunomodulators in acute experimental stroke. *Nat Med* 15: 192–199

Liu M, Xiao L, Liu S, Hu Y, Tian J, Gao G, Xie S, Guan Y (2013) Immunoregulation of myelin-specific CD4+ T cell response by neural stem/progenitor cells: role of prostaglandin E2. *J Neuroimmunol* 255: 32–38

Lone AM, Tasken K (2013) Proinflammatory and immunoregulatory roles of eicosanoids in T cells. *Front Immunol* 4: 130

de Los Reyes Jiménez M, Lechner A, Alessandrini F, Bohnacker S, Schindela S, Trompette A, Haimerl P, Thomas D, Henkel F, Mourão A *et al* (2020) An anti-inflammatory eicosanoid switch mediates the suppression of type-2 inflammation by helminth larval products. *Sci Transl Med* 12: eaay0605

MacKenzie KF, Clark K, Naqvi S, McGuire VA, Noehren G, Kristariyanto Y, van den Bosch M, Mudaliar M, McCarthy PC, Pattison MJ *et al* (2013) PGE(2) induces macrophage IL-10 production and a regulatory-like phenotype via a protein kinase A-SIK-CRTC3 pathway. *J Immunol* 190: 565–577

Mahanty S, Orrego MA, Mayta H, Marzal M, Cangalaya C, Paredes A, Gonzales-Gustavson E, Arroyo G, Gonzalez AE, Guerra-Giraldez C *et al* (2015) Post-treatment vascular leakage and inflammatory responses around brain cysts in porcine neurocysticercosis. *PLoS Negl Trop Dis* 9: e0003577

Maizels RM, Smits HH, McSorley HJ (2018) Modulation of host immunity by helminths: the expanding repertoire of parasite effector molecules. *Immunity* 49: 801–818

Matheu MP, Othy S, Greenberg ML, Dong TX, Schuijs M, Deswarte K, Hammad H, Lambrecht BN, Parker I, Cahalan MD (2015) Imaging regulatory T cell dynamics and CTLA4-mediated suppression of T cell priming. *Nat Commun* 6: 6219

McCullough L, Wu L, Haughey N, Liang X, Hand T, Wang Q, Breyer RM, Andreasson K (2004) Neuroprotective function of the PGE2 EP2 receptor in cerebral ischemia. *J Neurosci* 24: 257–268

Metallo CM, Gameiro PA, Bell EL, Mattaini KR, Yang J, Hiller K, Jewell CM, Johnson ZR, Irvine DJ, Guarente L *et al* (2011) Reductive glutamine metabolism by IDH1 mediates lipogenesis under hypoxia. *Nature* 481: 380–384

Narumiya S, Sugimoto Y, Ushikubi F (1999) Prostanoid receptors: structures, properties, and functions. *Physiol Rev* 79: 1193–1226

Neil JR, Johnson KM, Nemenoff RA, Schiemann WP (2008) Cox-2 inactivates Smad signaling and enhances EMT stimulated by TGF-beta through a PGE2-dependent mechanisms. *Carcinogenesis* 29: 2227–2235

Nono JK, Pletinckx K, Lutz MB, Brehm K (2012) Excretory/secretory-products of Echinococcus multilocularis larvae induce apoptosis and tolerogenic properties in dendritic cells *in vitro*. *PLoS Negl Trop Dis* 6: e1516

Norlander AE, Bloodworth MH, Toki S, Zhang J, Zhou W, Boyd K, Polosukhin VV, Cephus J-Y, Ceneviva ZJ, Gandhi VD *et al* (2021) Prostaglandin I2 signaling licenses Treg suppressive function and prevents pathogenic reprogramming. *J Clin Invest* 131: e140690

Oyesola OO, Shanahan MT, Kanke M, Mooney BM, Webb LM, Smita S, Matheson MK, Campioli P, Pham D, Früh SP *et al* (2021) PGD2 and CRTH2 counteract Type 2 cytokine-elicited intestinal epithelial responses during helminth infection. *J Exp Med* 218: e20202178

Pettipher R, Hansel TT, Armer R (2007) Antagonism of the prostaglandin D2 receptors DP1 and CRTH2 as an approach to treat allergic diseases. *Nat Rev Drug Discov* 6: 313−325

Pinto ML, Rios E, Duraes C, Ribeiro R, Machado JC, Mantovani A, Barbosa MA, Carneiro F, Oliveira MJ (2019) The two faces of tumor-associated macrophages and their clinical significance in colorectal cancer. *Front Immunol* 10: 1875

Prabhakaran V, Drevets DA, Ramajayam G, Manoj JJ, Anderson MP, Hanas JS, Rajshekhar V, Oommen A, Carabin H (2017) Comparison of monocyte gene expression among patients with neurocysticercosis-associated epilepsy, Idiopathic Epilepsy and idiopathic headaches in India. *PLoS Negl Trop Dis* 11: e0005664

Prodjinotho UF, Lema J, Lacorcia M, Schmidt V, Vejzagic N, Sikasunge C, Ngowi B, Winkler AS, Prazeres da Costa C (2020) Host immune responses during *Taenia solium* Neurocysticercosis infection and treatment. *PLoS Negl Trop Dis* 14: e0008005

Sakaguchi S, Yamaguchi T, Nomura T, Ono M (2008) Regulatory T cells and immune tolerance. *Cell* 133: 775−787

Saleem S, Kim YT, Maruyama T, Narumiya S, Dore S (2009) Reduced acute brain injury in PGE2 EP3 receptor-deficient mice after cerebral ischemia. *J Neuroimmunol* 208: 87−93

Sikasunge CS, Johansen MV, Willingham 3rd AL, Leifsson PS, Phiri IK (2008) *Taenia solium* porcine cysticercosis: viability of cysticerci and persistency of antibodies and cysticercal antigens after treatment with oxfendazole. *Vet Parasitol* 158: 57−66

Singh AK, Singh SK, Singh A, Gupta KK, Khatoon J, Prasad A, Rai RP, Gupta RK, Tripathi M, Husain N *et al* (2015) Immune response to *Taenia solium* cysticerci after anti-parasitic therapy. *Int J Parasitol* 45: 749−759

Sokolowska M, Chen LY, Eberlein M, Martinez-Anton A, Liu Y, Alsaaty S, Qi HY, Logun C, Horton M, Shelhamer JH (2014) Low molecular weight hyaluronan activates cytosolic phospholipase A2alpha and eicosanoid production in monocytes and macrophages. *J Biol Chem* 289: 4470−4488

Sorgi CA, Zarini S, Martin SA, Sanchez RL, Scandiuzzi RF, Gijon MA, Guijas C, Flamand N, Murphy RC, Faccioli LH (2017) Dormant 5-lipoxygenase in inflammatory macrophages is triggered by exogenous arachidonic acid. *Sci Rep* 7: 10981

Sotelo J (2011) Clinical manifestations, diagnosis, and treatment of neurocysticercosis. *Curr Neurol Neurosci Rep* 11: 529−535

Stein JV, Nombela-Arrieta C (2005) Chemokine control of lymphocyte trafficking: a general overview. *Immunology* 116: 1−12

Thomas PE, Peters-Golden M, White ES, Thannickal VJ, Moore BB (2007) PGE(2) inhibition of TGF-beta1-induced myofibroblast differentiation is Smad-independent but involves cell shape and adhesion-dependent signaling. *Am J Physiol Lung Cell Mol Physiol* 293: L417−L428

Uddin J, Gonzalez AE, Gilman RH, Thomas LH, Rodriguez S, Evans CA, Remick DG, Garcia HH, Friedland JS (2010) Mechanisms regulating monocyte CXCL8 secretion in neurocysticercosis and the effect of antiparasitic therapy. *J Immunol* 185: 4478−4484

Vatankhah A, Halasz J, Piurko V, Barbai T, Raso E, Timar J (2015) Characterization of the inflammatory cell infiltrate and expression of costimulatory molecules in chronic echinococcus granulosus infection of the human liver. *BMC Infect Dis* 15: 530

Verma A, Prasad KN, Cheekatla SS, Nyati KK, Paliwal VK, Gupta RK (2011) Immune response in symptomatic and asymptomatic neurocysticercosis. *Med Microbiol Immunol* 200: 255−261

Weissberg I, Wood L, Kamintsky L, Vazquez O, Milikovsky DZ, Alexander A, Oppenheim H, Ardizzone C, Becker A, Frigerio F *et al* (2015) Albumin induces excitatory synaptogenesis through astrocytic TGF-beta/ALK5 signaling in a model of acquired epilepsy following blood-brain barrier dysfunction. *Neurobiol Dis* 78: 115−125

White Jr AC, Coyle CM, Rajshekhar V, Singh G, Hauser WA, Mohanty A, Garcia HH, Nash TE (2018) Diagnosis and treatment of neurocysticercosis: 2017 Clinical Practice Guidelines by the Infectious Diseases Society of America (IDSA) and the American Society of Tropical Medicine and Hygiene (ASTMH). *Am J Trop Med Hyg* 98: 945−966

Wilson EH, Weninger W, Hunter CA (2010) Trafficking of immune cells in the central nervous system. *J Clin Invest* 120: 1368−1379

Winkler AS (2012) Neurocysticercosis in sub-Saharan Africa: a review of prevalence, clinical characteristics, diagnosis, and management. *Pathog Glob Health* 106: 261−274

Xie L, Choudhury GR, Winters A, Yang SH, Jin K (2015) Cerebral regulatory T cells restrain microglia/macrophage-mediated inflammatory responses via IL-10. *Eur J Immunol* 45: 180−191

Zakeri A, Hansen EP, Andersen SD, Williams AR, Nejsum P (2018) Immunomodulation by helminths: intracellular pathways and extracellular vesicles. *Front Immunol* 9: 2349

Zhang J, Rivest S (2001) Anti-inflammatory effects of prostaglandin E2 in the central nervous system in response to brain injury and circulating lipopolysaccharide. *J Neurochem* 76: 855−864